LUND UNIVERSITY

LTH

FACULTY OF ENGINEERING

Centre for Analysis and Synthesis

MSc in Chemical Engineering
Thesis in Organic Chemistry
KASM05

Synthesis of Organo-Iron(II) Complexes including N-Heterocyclic Carbene Ligation as Solar Cell Material.

Fulfilled by **Salim Charkas**

Supervised by **Samuel Persson**

Examined by **Ulf Nilsson**

June 2023, Lund

Table of Content

Acknowledgments

Special thanks to my supervisor, Samuel Persson, for guiding me through this thesis and making my lab work at the CAS as enjoyable as possible. It has been an absolute pleasure to work under your supervision.

Special thanks to Kenneth Wärnmark for giving me the opportunity to work on this exciting project. It has truly been a wonderful adventure to explore this field through your contributions in the form of released literature.

I also want to send my gratitude to the people in the Wärnmark group for your hospitality, generosity, and resourcefulness. It has been a great experience to be acquainted with you all.

Abstract

The push-pull design has been shown to increase DSC performance through the introduction of electron-withdrawing groups and electron-donating groups, usually on opposite far ends of the sensitizer. The scope of this thesis was to synthesize several *pre-N-heterocyclic carbene* ligand analogs that are inspired by the push-pull design in an attempt to investigate their susceptibility to Fe(II) complexation. Four *pre-N-heterocyclic carbene* ligands were synthesized followed by four complex attempts, where one homoleptic complex and one heteroleptic complex were successfully synthesized.

Acronyms and Abbreviations

MOS	Metal Oxide Semiconductor
HOMO	Highest Occupied Molecular Orbital
LUMO	Lowest Unoccupied Molecular Orbital
SOMO	Singly Occupied Molecular Orbital.
RT	Room Temperature
CB	Conduction Band
TM	Transition Metal
TMC	Transition Metal Complex
MeOH	Methanol
EtOH	Ethanol
DIPA	Diisopropylamine
LDA	Lithium Diisopropylamide
TFA	Trifluoroacetic Acid
THF	Tetrahydrofuran
TMS	Trimethylsilyl
KO*t*-Bu	Potassium Tert-Butylate
n-BuLi	*n*-Butyllithium
$B_2(Pin)_2$	Bis(pinacolato)diboron
KOAc	Potassium acetate
EA	Ethyl Acetate
Et_2O	Diethyl Ether
PE	Petroleum Ether
DCM	Dichloromethane
DMF	Dimethylformamide
TLC	Thin Layer Chromatography
^{1}H NMR	Proton Nuclear Magnetic Resonance

1. Introduction

1.1. Background

The endeavor to find cheap, renewable, and abundant energy to meet humanity's energy demands today and, in the future, has become one of the most urgent tasks of modern times. The reason is partly because of the rapid growth in the human population, technology, industry, and living standards in the past couple of decades, leading to a continued increase in energy demands [1]. The main reason, however, is the binary problem that transpires with using fossil fuel as the leading source of energy as of the current trend; the limited quantity and the emissions released. Fossil fuels are a limited resource. The discovered cache of oil and natural gas available for extraction is estimated to be depleted by the year 2055 according to projections based on current and future energy expenditure trends [2]. Therefore, substitutions need to be established well in advance to avoid an energy crisis in the ever-nearing future. As for the emissions, fossil fuel combustion releases greenhouse gasses that compromise the environment and the consequences will inevitably change the landscape as we know it today, with potentially devastating and irreversible ecological, geological, meteorological, oceanological, and epidemiological effects [3], [4], [5].

Sustainable energy sources that do not pose any of the abovementioned issues are wind, hydroelectric, nuclear, and solar, with the former two being indirectly procured from solar energy. The Sun is the largest and most abundant energy source available. The solar energy that continuously radiates on the earth's surface is 10,000 times greater than the current energy demand, making the harvesting of solar energy the option with the largest potential [6].

1.2. Dye-sensitized Solar Cell

Solar cells generate solar radiation to energy by absorbing sunlight and converting it into electricity. Dye-sensitized solar cells (DSCs), also known as Grätzel cells, named after the chemist Michael Grätzel, are a subtype of solar cells that are based on dyes as photosensitizers and redox-active electrolytes, inspired by the photosynthetic process in plants. Grätzels and O'Regan's innovative DSC make-up in the early 90s gave an average efficiency rate above 7 % which at the time was about 10 magnitudes higher than any other previously developed DSC and this sparked a large amount of interest in the development of DSCs [7]. Grätzel accomplished this by introducing an organo-Ru(II) complex as the sensitizer. The substitution of ZnO to a mesoporous TiO_2 was also a noteworthy implementation as this MOS is one of the most utilized variants even to this day [7].

1.2.1. Principle of DSCs

The operation of the DSC can be broken down into four steps (see Figure 1) and each step is contingent on the electrons transitioning from higher energy levels to lower energy levels as that

is the driving force after excitation. (1) The initiation of the process through the absorption of incident light (*hv*) by the sensitizer (D) at its ground state (GS), resulting in the excitation of an electron to a higher energy level (D^*). (2) In the excited state, the sensitizer is oxidized (D^+) as it can donate an electron to the conduction band of the MOS that it is adsorbed on. This gives rise to an electrical current that travels through the extrinsic circuit and thus generates electricity. (3) The electrons reach the cathode and will reduce the redox electrolyte. (4) The redox electrolyte subsequently reduces (regenerates) the D^+ back to its original state (D), thus completing the circuit [8], [9].

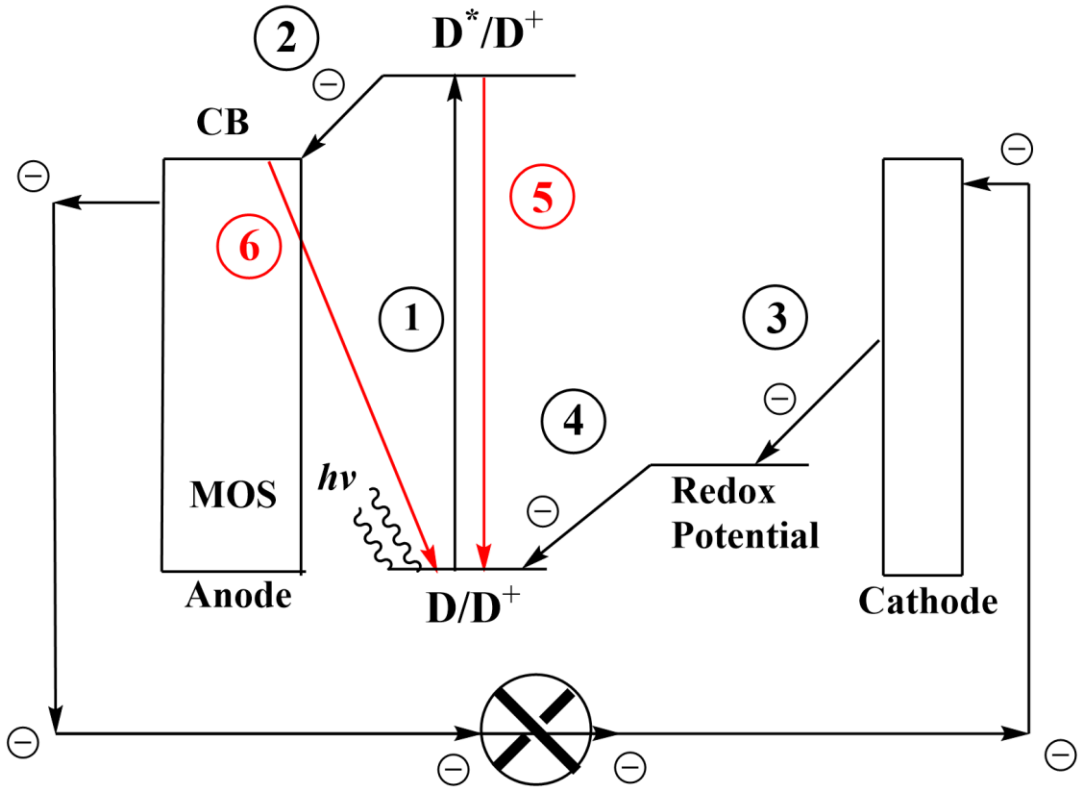

Figure 1: An overview of how a DSC operates (steps 1-4) and how the efficiency is decreased (steps 5-6).

This thesis will hereon focus on the theory and synthesis of the sensitizer.

1.3. The Sensitizer

There are two relevant factors that should be mentioned that can lower the efficiency in a DSC system and they are highlighted in step 5 and 6 in Figure 1. (5) The lifetime of the D* can be too short for the electron injection to happen and this leads to the relaxation of D* to D before electron injection to the MOS, thus decreasing the overall efficiency. The excited state lifetime in TMCs can be achieved with the implementation of strong σ-donors (more on that in section 1.3.1.) [8]. (6) Recombination of an electron from the CB to the D^+. The electron contributed to the CB will unfavorably regenerate the D^+ back to D instead of the electrolyte and ultimately not provide the CB with a net electron [8].

The solution to combat the efficiency problems mentioned above has been to design the sensitizers in a so-called push-pull fashion, which have shown to make sensitizers more efficient [9], [10], [11]. One way to implement the push-pull design is to use electron-withdrawing groups (EWGs) as electron acceptors and electron-donating groups (EDGs) as electron donors, usually on opposite sides of the sensitizer, where the EWGs are closer to the MOS surface. The suggested notion is that by having EWGs close to the anchor and EDGs at the far end of the sensitizer would lead to a greater electron density close to the MOS surface and greater hole density around the EDGs during excitation and thus make recombination less prevalent [9], [10]. In molecular orbital (MO) theory, it would mean that the HOMO of the sensitizer would largely be localized around the EDGs and the unoccupied MO (i.e., LUMO) would be largely localized close to the EWGs when the sensitizer is excited. This gives rise to an intramolecular charge transfer that is directed from the EDGs towards the EWGs, and this would generally leave the SOMO less accessible to regeneration from the MOS due to a decrease in orbital overlap [10].

Furthermore, there are multiple requisites that a sensitizer needs to fulfill to be considered a viable option. It needs to have a wide absorption spectrum that would ideally include all wavelengths below 920 nm (up to infrared light) as wavelengths within this region have in general shown the most intense absorption peaks in spectroscopic analyses due to water and CO_2 absorbing infrared light [6]. It needs to have an anchoring group that adsorbs to the MOS, this is done with a functional group such as carboxylates [8]. The adsorbed sensitizers should also create a monolayer on the surface of the MOS and not aggregate or dimerize. The sensitizer needs to have a long lifespan, which is assessed on the sensitizer's thermal and electrochemical stability and the energy level of its excited state needs to eclipse that of the conduction band edge to allow electron injection into the MOS. The sensitizers that have been synthesized yet are nowhere near working optimally in a fully functioning DSC [6], [8].

1.3.1. Transition Metal Complexes and N-Heterocyclic Carbenes

TMCs have been investigated extensively as sensitizers in DSCs. They consist of a central metal with ancillary ligands and at least one anchoring ligand. The light absorption is made possible by the metal-to-ligand charge transfer (MLCT) states and can be modified by altering or extending the ligands as well as using different metals. The most researched and efficient TMCs are based on second- and third-row TMs, such as Ru, Ir, and Os due to their widely absorbing spectrums, appropriate GS and excited state energy levels, a relatively long-lived MLCT and excellent durability and lifespan [6], [12]. The problem however is that the TMs mentioned are scarce, toxic, and are not feasible to incorporate at an industrial scale [12], [13]. Fe belongs to the same group (8) as Ru and Os in the periodic table and has the benefit of being the most abundant and cheap TM available. The hurdle with Fe compared to the other mentioned TMs is overcoming the shorter MLCT lifetime due to a low-lying metal-centered (MC) high spin state [13]. Ru complexes having larger orbital splitting than Fe complexes (Figure 2) and one explanation to this is that this facilitate a rapid disengagement of the MLCT into the MC states which renders the sensitizers unable to inject electrons into the CB of the MOS [12], [13].

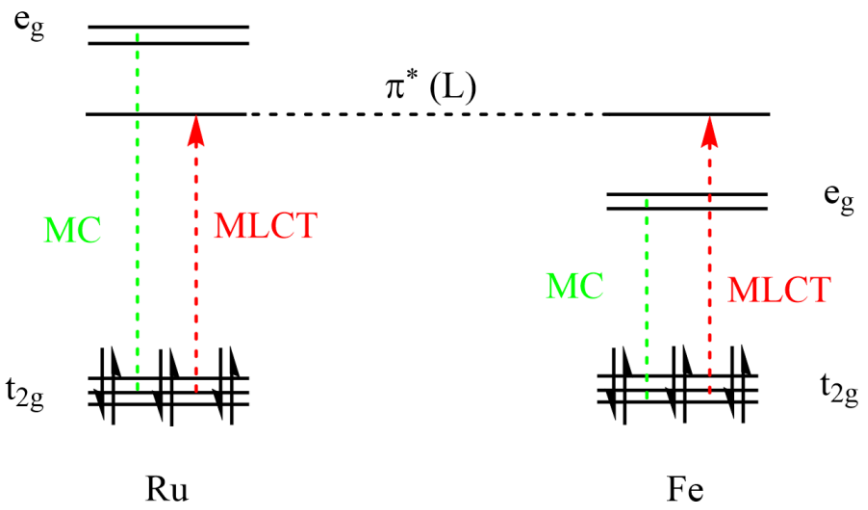

Figure 2: An overview of the MLCT and MC transitions of Fe and Ru complexes, where the MC states in the Fe complex are low-lying relative to Ru.

The measures to prolong the MLCT states in Fe complexes usually involve lowering the π^* orbitals or by raising the e_g orbitals. π^* is ligand-dependent and can be lowered by expanding the conjugated π-system in the ligand, this method is however not ideal due to the MLCT state being the photoactive state and lowering it too much would limit the driving force of the CB injection. The destabilization of the e_g orbitals can be done by the introduction of N-heterocyclic carbenes (NHCs) due to their strong σ-donation which has been shown to delay the MLCT decay [12], [13], [14].

Carbenes are normally unstable in ambient conditions as they only have two σ-bonds and six valence electrons, which means that they have an unfilled octet [15]. Carbenes are stable in NHCs due to the presence of the two neighboring electron-donating nitrogens via inductive and mesomeric effects as illustrated with imidazol-2-ylidene in Figure 3 [15]. There are numerous NHC-based ligands in metal complexes, this thesis will reference NHC as being imidazol-2-ylidene to keep the text more coherent and relevant to the work as it was the only NHC used.

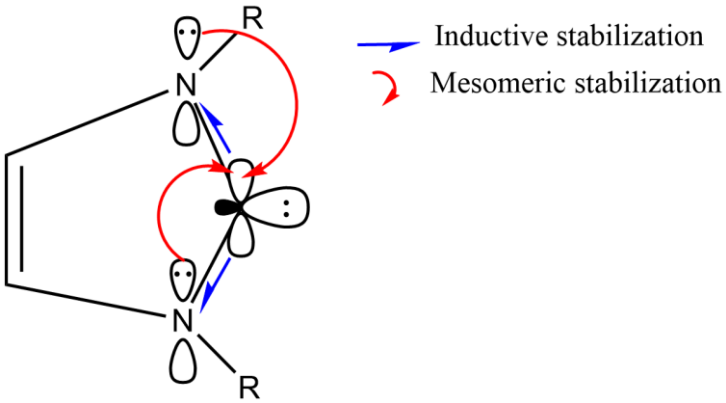

Figure 3: an overview of the stabilization of the carbene in imidazol-2-ylidene. The adjacent nitrogens stabilize the carbene through mesomeric and inductive effects.

In the case of Fe, the strongly σ-donating electrons in the lone pair of the NHCs are coordinated to the Fe d-orbitals (d_{z^2} and $d_{x^2-y^2}$) and this extra electron density results in the destabilization of the e_g orbitals to higher energy levels [12], [16].

1.3.2. Fe(II)NHC Complexes

The inspiration to combine Fe with NHCs came from the great success in destabilizing the MC states observed with RuNHC complexes, the main one being **CX0** in Figure 4 [17], [18]. This led to the complexation of the tridentate ligand with Fe(II) to get the Fe(II)NHC complex (**CX1**). **CX1** showed an MLCT lifetime of 9 ps via transient absorption spectroscopy, an increase of almost two orders of magnitude in comparison to the referenced Fe(II) bis-terpyridine complex [17].

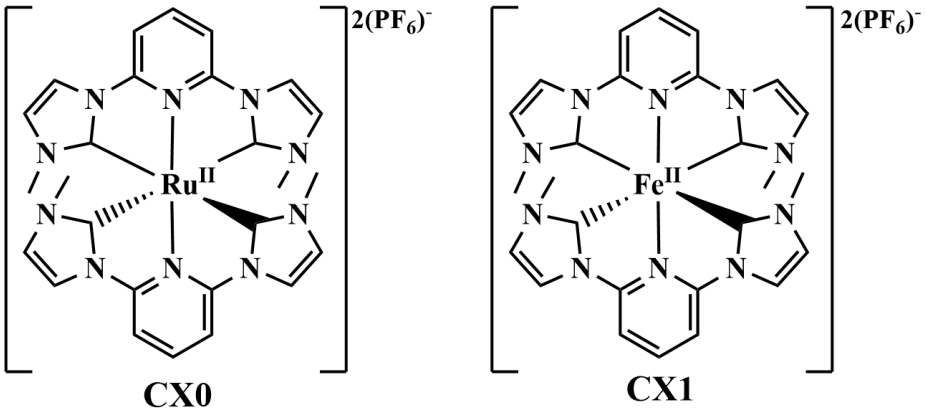

Figure 4: Early contributions towards Fe(II)NHC complexes with the synthesis of **CX1**. Inspiration came from the Ru complex (**CX0**).

The pyridines in the complexes act as electron acceptors to enable the MLCT excitation, resulting in a tridentate ligand.
The success of **CX1** led to numerous modifications to further improve and explore new analogs as potential photosensitizers. Some of the explored analogs are presented in Figure 5 and they include the extension of the π-system (**CX2**), the substitution of a pyrazine ring instead of the pyridine ring (**CX3**), and the introduction of carboxyl groups as anchoring groups and EWGs (**CX4**) [14].

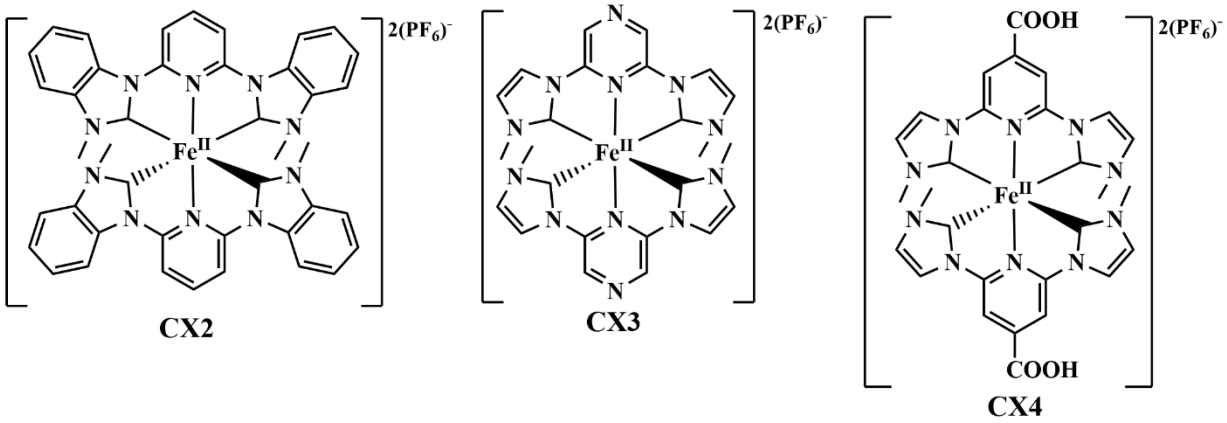

Figure 5: Early contributions towards the Fe(II)NHC. **CX2**, **CX3** and **CX4** are analog complexes, based on the parent complex, **CX1**.

All the complexes in Figure 5 showed an increase in MLCT lifetime compared to **CX1** [14], [19]. An analog of **CX2** with carboxyl groups on the para position in the pyridines was implemented to make the complex feasible for DSC sensitization, but the resulting complex showed a low photoconversion efficiency (PCE) of 0.03 % [14], [20]. **CX4** showed an MLCT lifetime of 16.5 ps and a PCE of 0.66 %, with measurements indicating that the low efficiency was due to rapid recombination [20], [21], [22].

Furthermore, push-pull designs have been attempted with Fe(II)NHC complexes, highlighted in Figure 6. Recently designed complexes having both the EWGs and EDGs on the same ligand showed relatively low PCE at around 0.1% (**CX5** and **CX6**). Complexes with a directional excitation design, where the push-pull groups were on separate ligands, on the para position in the pyridine rings (**CX7** and **CX8**) showed substantially higher PCE of 1.3 % [20], [22].

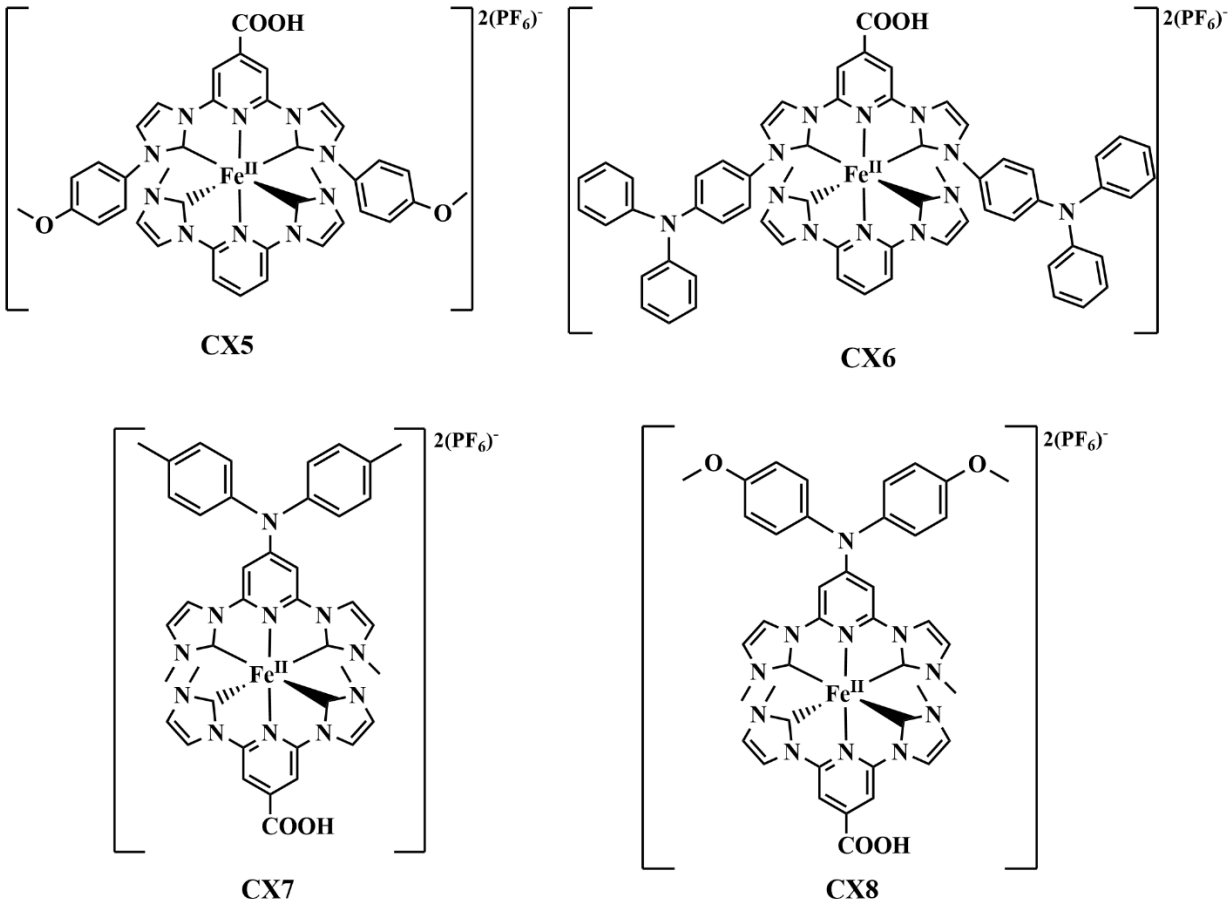

Figure 6: Earlier contributions towards Fe(II)NHC complexes with push-pull designs. **CX5** and **CX6** have the push-pull groups on the same ligand, while **CX7** and **CX8** have them on different ligands on the para position in the pyridines.

This has led us to try synthesizing pre-NHC ligands with push-pull design and investigate their susceptibility for complexation in the attempt to incorporate them in Fe(II) complexes with the same design as **CX7** and **CX8**.

2. Thesis Scope

This work consists of synthesizing pre-NHC ligands based on **CX1** with incorporated push-pull design in the para position on the pyridines and we want to investigate their susceptibility to Fe(II) complexation (Figure 7). All the pre-NHC ligands within the scope of this thesis are drawn in Figure 8.

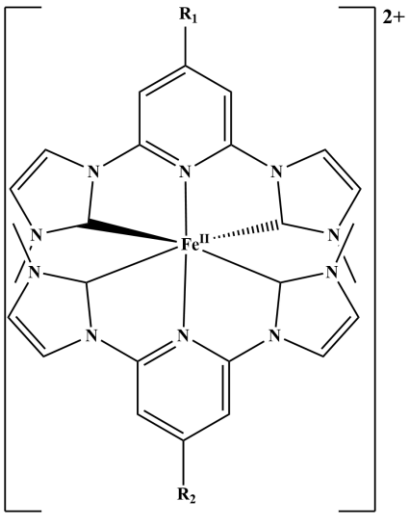

FeNHC 1

Figure 7: The octahedral complex of Fe(II)NHC with two NHC ligands that can be either identical (homoleptic) or different (heteroleptic) depending on the R groups.

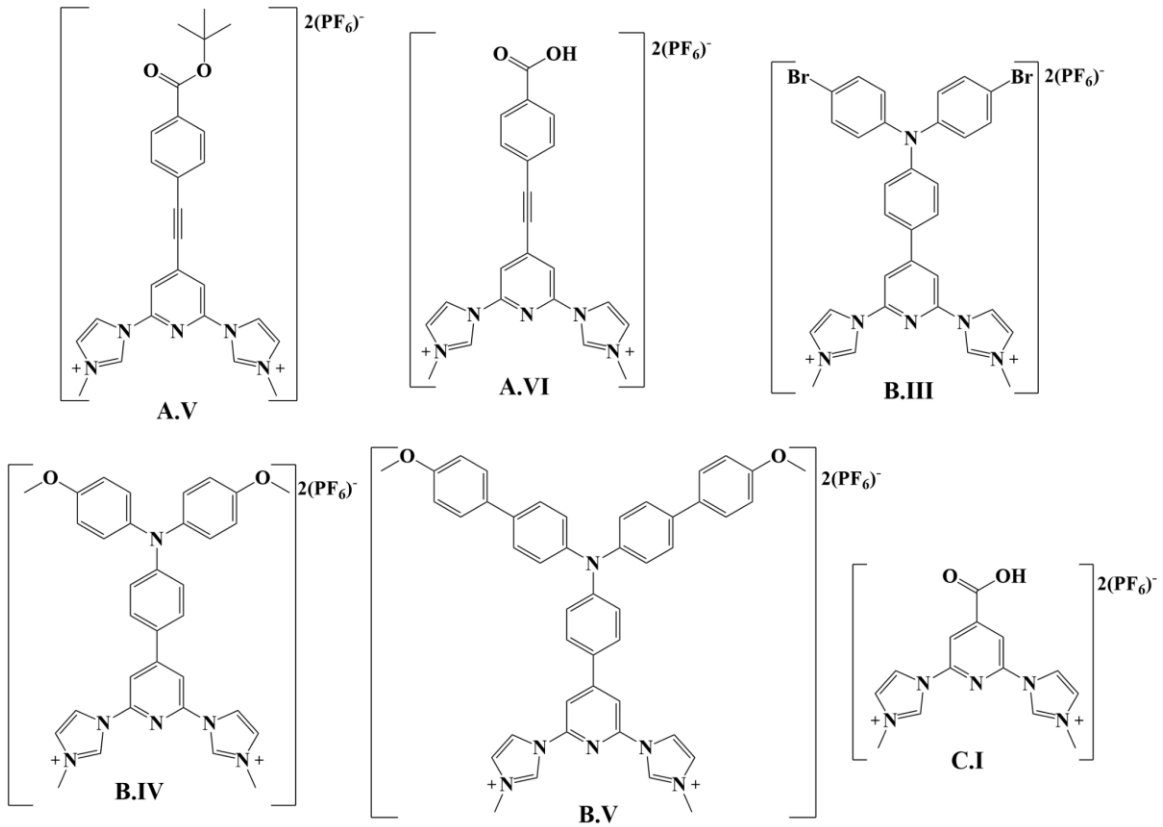

Figure 8: An overview of the chemical structures of all the pre-NHC ligands that were planned to be synthesized and potentially complexed to Fe(II). The ligands are all positively charged due to the imidazolium groups and PF_6^- was used as the counterion.

2.1. Acetylene and Hole-Acceptor Projects

Ligand A (**A.VI)** and its protected analog, **A.V**, are incorporated with an acetylene group with the purpose to investigate whether it would increase the efficiency, incorporated acetylenes could also lead to an increase in light absorption in the red part of the spectra [14], [23]. **A.V** and **A.VI** are considered pulling groups (with EWGs) and have been synthesized before by our group (among other acetylene ligand moieties), but complexation to Fe(II) with **A.V** and **A.VI** has never been successful. The plan in this thesis was to re-synthesize the ligands and attempt the complexation again under different conditions.

Moreover, the chemical structure of ligand B (**B.III**) and its analogs (**B.IV,** and **B.V**), were inspired by K. Oum et al. and Y. Hao et al., aromatic amines are often used as EDGs and have been shown to increase efficiency as hole acceptors in organic dyes [24], [25]. Therefore, investigating whether **B.III** and its analogs can be synthesized and complexed to Fe(II) is an interesting prospect.

2.2. Objectives

The primary objectives are to synthesize the pre-NHC ligands **A.V**, **A.VI,** and **B.III** in an attempt to complex them to Fe(II) homoleptically (Scheme 1) and heteroleptically in a push-pull fashion by combining **B.III** with either **A.V** or **A.VI** in a complexation attempt. The secondary objectives are to synthesize **B.IV** and **B.V** and complex them to Fe(II) if enough time is available. Depending on the success of the ligand syntheses and complexation attempts mentioned above, **C.I** could be considered to be synthesized and used as an alternative in a heteroleptic complexation attempt with either **B.III**, **B.IV** and **B.V**. **C.I** is the tridentate ligand used in **CX4** and has been used extensively as an anchoring ligand in many groups, including ours [12], [14], [22].

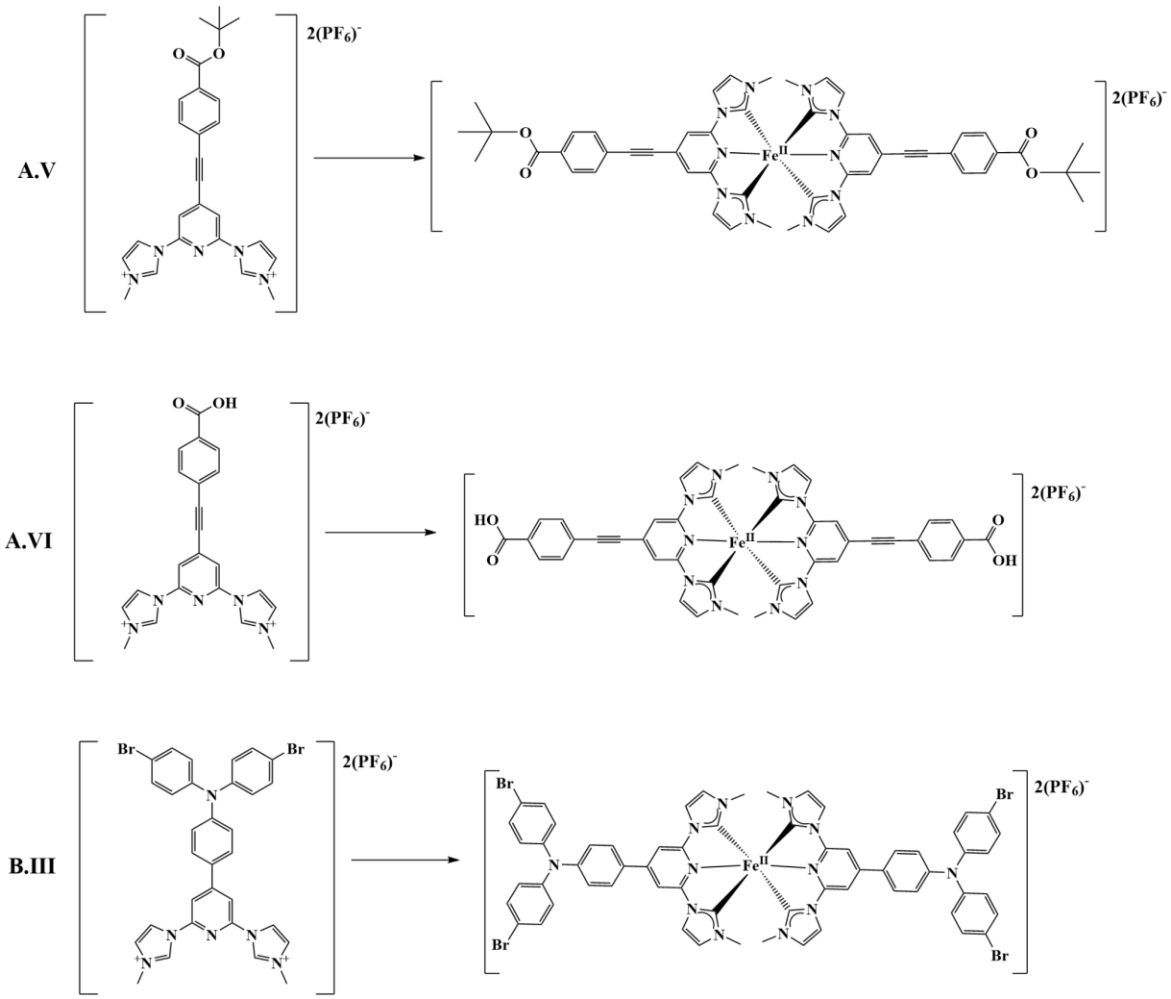

Scheme 1: Ligands **A.V**, **A.VI,** and **B.III** and their corresponding homoleptic complex to Fe(II).

The objectives are purposely formulated this way to answer the following research questions:

- Is it possible to complex **A.V** and **A.VI** to Fe(II)?
- Is it possible to synthesize **B.III** and complex it to Fe(II)?
- Is it possible to synthesize **B.IV** or **B.V** and complex them to Fe(II)?

Answering these questions will hopefully contribute to the long-term goal of this research field; to develop and improve the efficiency of Fe(II)NHC complexes due to the commercial potential and abundance of Fe.

3. Results and Discussion

Subsection 3.2., Subsection 3.3. and Subsection 3.5. present the synthesis of ligands A, B and, C respectively. The methylation step (synthesis of **A.V** and **B.III**) is presented in Subsection 3.4. due to both reaction conditions being identical and relevant for both pathways. Subsection 3.6. is solely complex related. All synthesized products were confirmed by ^{1}H NMR and the spectrums are available in Subsection 7.1..

3.1. Formation of 2,6-Diimidazole-4-Iodo-Pyridine

2,6-diimidazole-4-iodopyridine (**Im-Pyr-Im**) was the NHC backbone of ligands A and B. Therefore, the synthesis of **Im-Pyr-Im** is presented and discussed in this subsection. The chemical structure and reaction conditions are illustrated in Scheme 2.

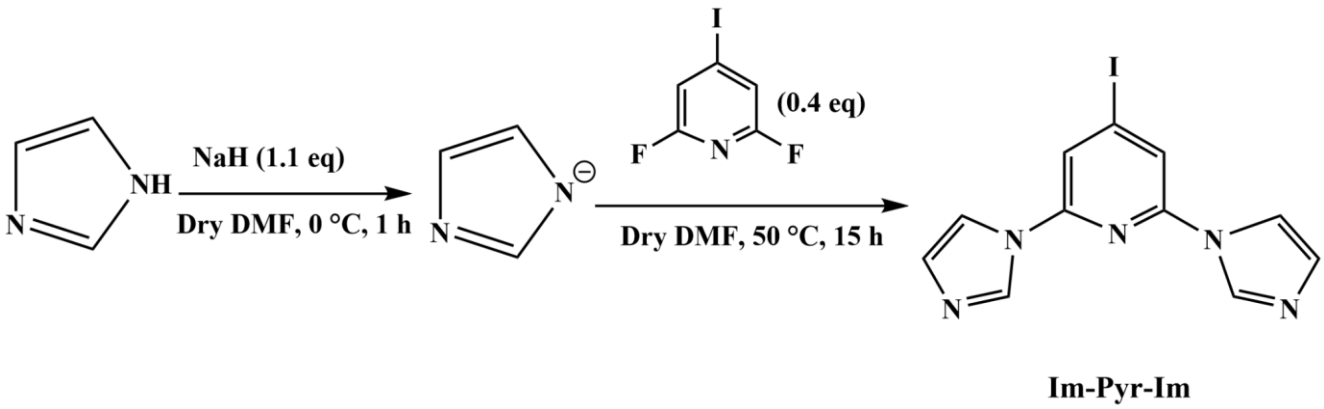

Scheme 2: Chemical structure and the two-step reaction conditions for the synthesis of **Im-Pyr-Im**.

The reaction is initiated by the hydride deprotonating imidazole to form H_2 gas and imidazolate to increase the nucleophilicity of the reactant. The hydrogen most susceptible to attack is the one bound to the nitrogen due to its acidity and the stability of the structure due to the delocalization of the negative charge between both nitrogens [26]. A good indicator that the reaction was working was the formation of H_2 gas on the surface of the mixture. The addition of 2,6-difluoro-4-iodo-pyridine opened for nucleophilic aromatic substitution (S_NAr) on both ortho carbons by the imidazolate. The most electron-deficient carbons on the ring are the ortho ones because of their highly electronegative neighbors and although iodide is a better leaving group than fluoride, the nucleophilic attack still favors both ortho positions due to the nitrogen being able to accept the incoming electron density from the imidazolate. The reaction was conducted once, and **Im-Pyr-Im** was obtained with a yield of 74 %.

3.2. Synthesis Pathway of Ligand A

The synthesis pathway of the pre-NHC ligands, **A.V** and **A.VI**, is presented in this subsection. The procedures were already established by our group, and they were for the most part precisely followed. The synthesis pathway is illustrated in Scheme 3.

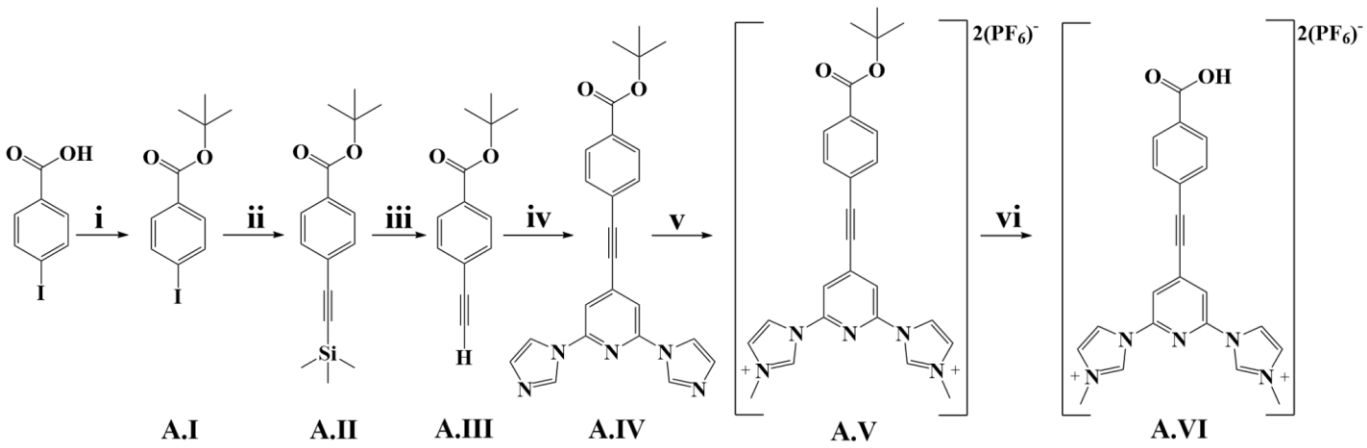

Scheme 3: Synthesis pathway of ligand A. The synthesized compounds are named from **A.I** to **A.VI** chronologically. The reaction conditions are named from **i** to **vi** chronologically. **i**: a) $SOCl_2$, 75 °C, 30 min.
b) KO*t*-Bu, DCM, 18 h, RT. **ii**: $Pd(PPh_3)_2Cl_2$, CuI, Et_3N, TMS-acetylene, 18 h, RT. **iii**: KF, DMF, H_2O, 40 min, RT. **iv**: **Im-Pyr-Im**, $Pd(PPh_3)_2Cl_2$, CuI, DIPA, DMF, 18 h, RT. **v**: a) MeI, DMF, 1.5 h, 130 °C. b) KPF_6. **vi**: a) TFA, DCM, RT, overnight. b) KPF_6.

3.2.1. Formation of Acid Chloride Followed by Esterification

As previously mentioned, carboxylates (or other anchoring functional groups) are necessary for the complex to adsorb to the MOS. Usually, to protect a carboxyl group it is converted into an ester as this will prevent the group from engaging in the cross-coupling reactions later in the synthesis pathway. The conversion to an ester would also decrease the polarity of the molecule, which should increase its solubility in organic solvents and make purification more convenient. Therefore, 4-iodo-benzoic acid (starting material) was converted to an ester in this two-step reaction to enable the protection of the carboxyl group. The reaction conditions were in accordance with reaction **i** in Scheme 3. The average yield was 73 %.

The carboxylic acid is in the first reaction step subjected to $SOCl_2$ and catalytic DMF to convert the carboxyl group into a more reactive acid chloride. The suggested mechanism is initiated by DMF, where the carbonyl oxygen nucleophilically attacks $SOCl_2$, expelling a Cl^- in the process. The following intermediate is then nucleophilically attacked on the imine carbon by the eliminated Cl^- and this leads to the elimination of SO_2 and Cl^- and the formation of the Vilsmeier reagent as depicted in Scheme 4. The Vilsmeier reagent is attacked on the imine carbon by the carboxylic acid and after charge rearrangements the Cl^- is liberated. The Cl^- will in the last mechanism step attack the carbonyl carbon and form the acid chloride and expel a DMF molecule that can engage in another catalytic cycle [27].

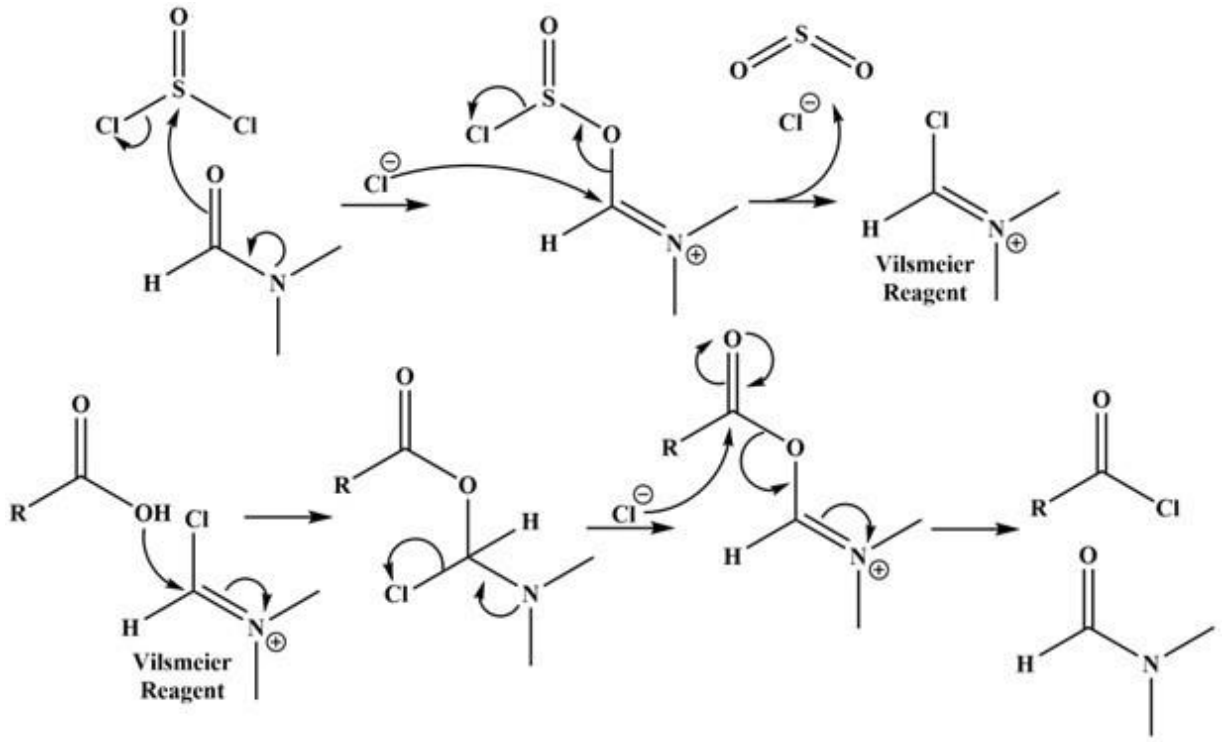

Scheme 4: The formation of acid chloride from a carboxyl acid catalyzed by DMF. The Vilsmeier reagent intermediate interacts with the carboxylic acid to obtain the acid chloride product and a DMF molecule. The formed DMF can thus engage in another catalytic cycle.

The chloride is easily replaced by reacting the acid chloride with an alkoxide ($^{-}$O*t*-Bu), which will make a nucleophilic attack on the carbonyl carbon and eliminate the chloride, thus obtaining a *t*-butyl ester [27].

3.2.2. Sonogashira Coupling and Desilylation

Compounds **A.II** and **A.IV** were both synthesized by utilizing Sonogashira coupling (**ii** and **iv**). The Sonogashira coupling can be performed under various conditions, the chosen conditions still gave a reasonably good yield and other conditions were thus not considered. The reaction mechanism is not fully understood but does involve a Pd(0) catalyst and a Cu(I) co-catalyst (see Scheme 5) [28].

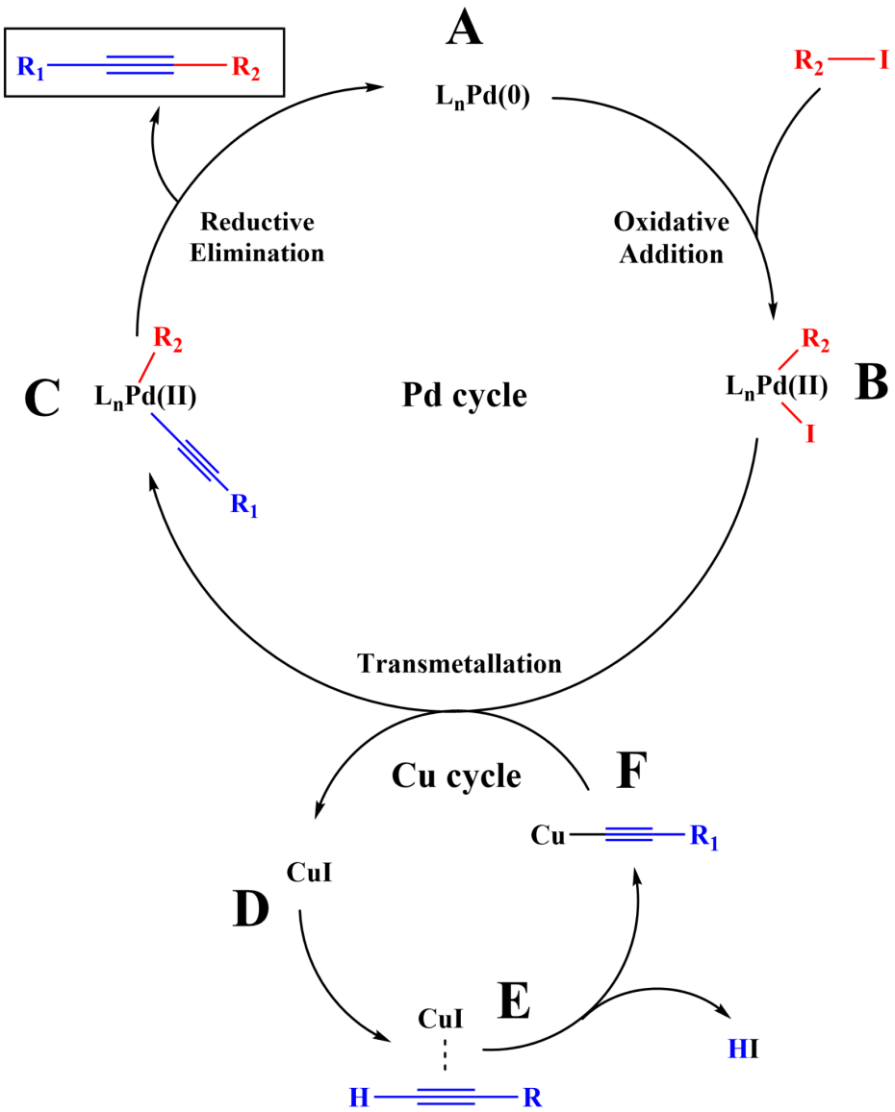

Scheme 5: An overview of the Sonogashira coupling mechanism including a Pd(0) and Cu(I) catalyzed cycles.

The precatalyst is reduced from Pd(II) to Pd(0) (A) which may be facilitated in the presence of an amine-base [28]. The Pd cycle starts with the oxidative addition of the aryl halide giving complex B. At the same time, the Cu cycle generates complex F by the coordination of CuI towards the π-bond of the terminal alkyne (E), which increases the acidity of the alkyne, resulting in its deprotonation and the formation of a Cu-acetylene complex. The transmetallation involves complex F and B and results in a double displacement, where the acetylene is exchanged for the halide on the Pd, resulting in the regeneration of the CuI species and the formation of complex C. Lastly, the product is formed by reductive elimination and Pd(0) is thus regenerated [28], [29].

Both reactions (**ii** and **iv**) were performed twice, and the average yields were 64 % for **ii** and 81 % for **iv**. One of the **iv** reaction attempts didn't generate any product and the reason is possibly due to improper degassing of the solvent, which may have led to oxidation of the Pd from oxygen and consequently to the homocoupling of **A.III** (Hay coupling) [30]. Using TMS-acetylene to synthesize an acetylene group to the ligand is an appropriate approach as this reagent is relatively safe and a liquid in ambient conditions, while acetylene on its own is an explosive gas [31].

The TMS was later removed in reaction **iii** and consisted of a simple deprotection step involving KF as a F^- source with a yield of 68 % (see the mechanism in Scheme 6).
TMS is a common protecting group of hydroxyls but also protects acetylenes [32]. F^- ions in the solution will in a S_N2 reaction attack Si in TMS and substitute the expelling acetylene anion. The acetylene anion will in turn deprotonate water to get the terminal acetylene (Scheme 2). This reaction is based on the strong affinity that silicone has for highly electronegative elements and the stability of the acetylene anion [31].

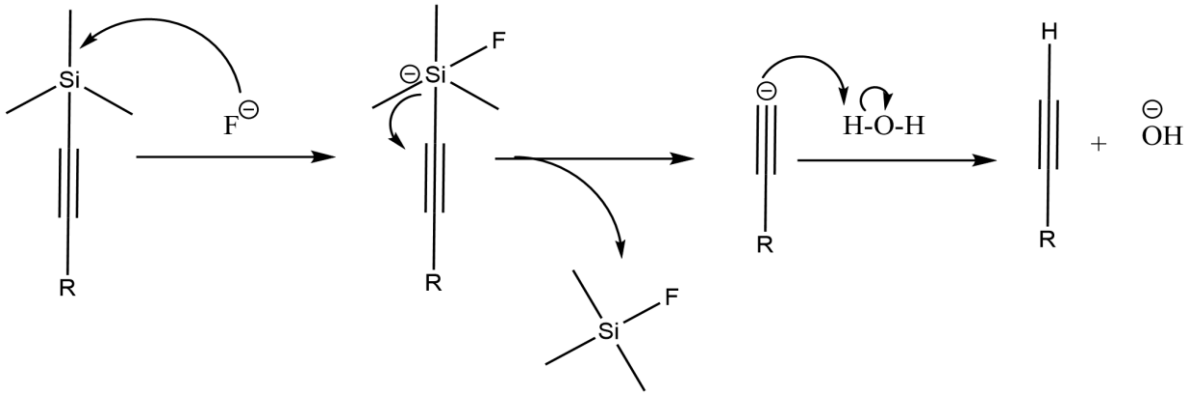

Scheme 6: Mechanism of desilylation of TMS-acetylene initiated by fluoride ion.

3.2.3. Ester Hydrolysis

Compound **A.V** was deprotected in reaction **vi**, giving **A.VI**. TFA is a strong acid effective in the hydrolysis of esters. The mechanism (Scheme 7) most likely involves the protonation of the carbonyl oxygen lone pair by the TFA due to the resonance making it more nucleophilic. After electron rearrangement, the *t*-butyl cation is expelled, giving a carboxyl group as the final product [33]. The *t*-butyl cation can further react with trifluoroacetate to form a isobutene and TFA, which can engage in another catalytic cycle. The yield was 86 %.

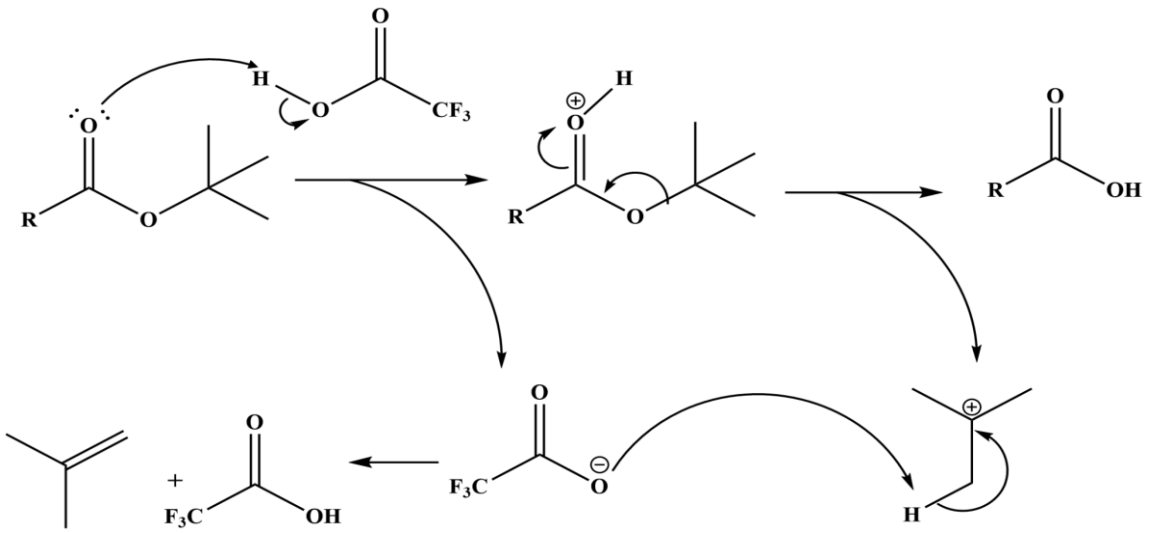

Scheme 7: The deprotection of the ester to form a carboxyl group via hydrolysis catalyzed by TFA. The byproducts, *t*-butyl cation and trifluoroacetate, engage in a reaction to form isobutene and a TFA molecule that can engage in another catalytic reaction.

3.3. Synthesis Pathway of Ligand B

The chemical structure of **B.III** and analogs were inspired by K. Oum et al. and the pathway consisted of three syntheses to get the pre-NHC ligand, **B.III** [24]. The synthesis pathway is depicted in Scheme 8. The synthesis of the analog compounds, **B.IV** and **B.V** (Figure 5), were never attempted due to a lack of time.

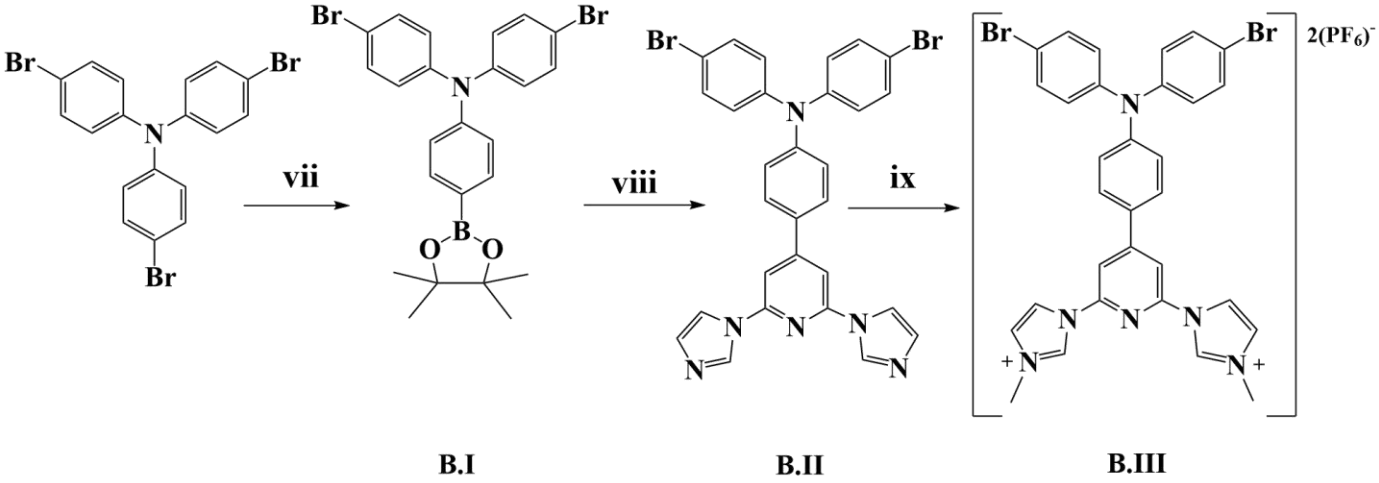

Scheme 8: Synthesis pathway of ligand B. The synthesized compounds are named from **B.I** to **B.III** chronologically and the reaction conditions are named from **vii** to **ix** chronologically. **vii**: $B_2(Pin)_2$, $Pd(dppf)Cl_2$, KOAc, 1,4-dioxane, 24 h, 110 °C. **viii**: **Im-Pyr-Im**, $Pd(PPh_3)_4$, K_2CO_3(1 M), Toluene:EtOH = 5:1, 70 °C, 18 h. **ix**: a) MeI, DMF, 1 h, 130 °C, b) KPF_6.

3.3.1. Miyaura Borylation

Miyaura borylation is a reaction that allows the formation of boron esters in place of a vinyl- or aryl halide. The reaction is Pd-catalyzed (Scheme 9) and starts with the oxidative addition of the aryl halide onto the Pd, oxidizing it in the process. The base ($^-$OAc) replaces the halide on the Pd via a ligand exchange [34]. Carboxylate bases are key in this reaction as other bases generally do not show full conversion and thus lower yield [35]. B_2pin_2 engages in the transmetallation process, where one boronic ester is exchanged with $^-$OAc on the Pd in basic conditions. Finally, the aryl boronic ester is reductively eliminated as the Pd(0) is regenerated [34].

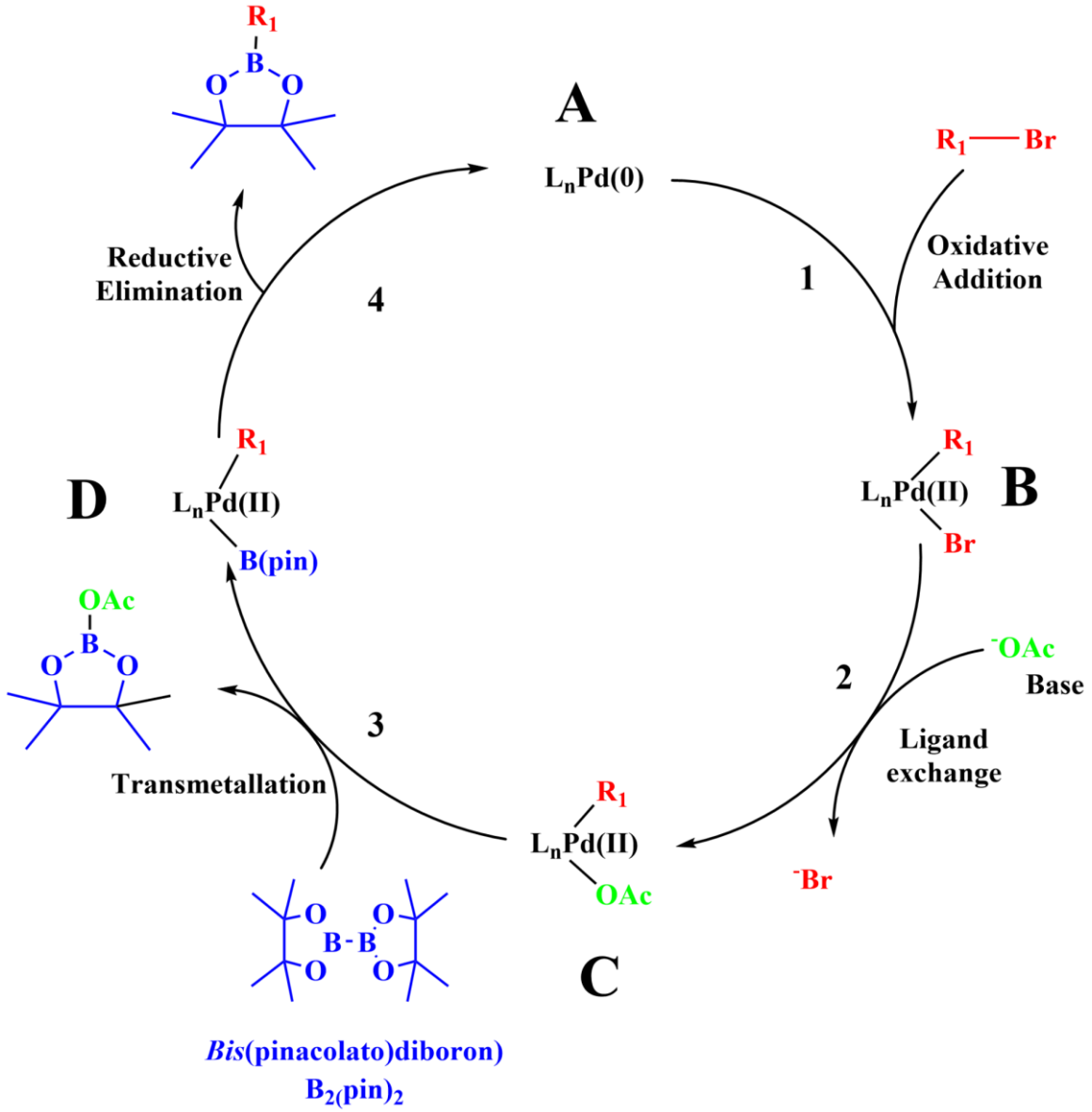

Scheme 9: An overview of the Miyaura borylation mechanism catalyzed by $L_nPd(0)$. 1) Oxidative addition of tris(4-bromophenyl)amine. 2) Halide exchanged for the base on the Pd(II). 3) Transmetallation of boron ester onto the Pd(II) catalyst. 4) Reductive elimination of **B.I**.

B.I was opted to be synthesized by the conditions in reaction **vii**, which was successful with an average yield of 33 %. The obtained yields were significantly lower than the yields reported in the literature [36].

Unreacted starting material, tris(4-bromophenyl)amine (TBPA), was isolated in both batches and the reason is most likely due to the same TBPA engaging in the cross-coupling up to three times as it has three bromides that are susceptible to borylation. This basically meant that one TBPA potentially was consuming more bis(pinacolato)diboron than what was intended and leading to unreacted TBPA. One solution would be to use a starting material with an iodide in place of one of the bromides (Bis(4-bromophenyl)-4-iodoaniline). Iodides usually have a higher reaction rate than bromides in other cross-coupling reactions and this could increase the selectivity of the borylation and thus increase the yield [37]. Another possible reason for the low yield could be

explained by the purification via column chromatography. **B.I** smeared heavily throughout the collected fractions, this meant that some **B.I** would get stuck in the column or elute together with side products, making isolation difficult. N. Oka et al. have reported that low yields are common with aryl boronic esters/acids species in silica gel and presented two consistent solutions to the problem; (1) The usage of a longer diboron ester as a reagent and (2) the pre-treatment of silica gel with boric acid before column chromatography [38]. None of these measures were ever explored as this information became known after both synthesis attempts.

3.3.2. Suzuki-Miyaura Coupling

The Suzuki-Miyaura coupling is used to form a C-C bond by reacting a halide with an organoborane species using a base and Pd(0) as a catalyst (Scheme 10). The Pd catalysis cycle starts as described above with the oxidative addition of the organohalide substituents, followed by the base-halogen exchange (metathesis) on the Pd(II). The transmetallation substitutes the base with the second R group on the Pd. Reductive elimination gives the C-C species and Pd(0) that can engage in another catalytic cycle [29]. The average yield was 74 %.

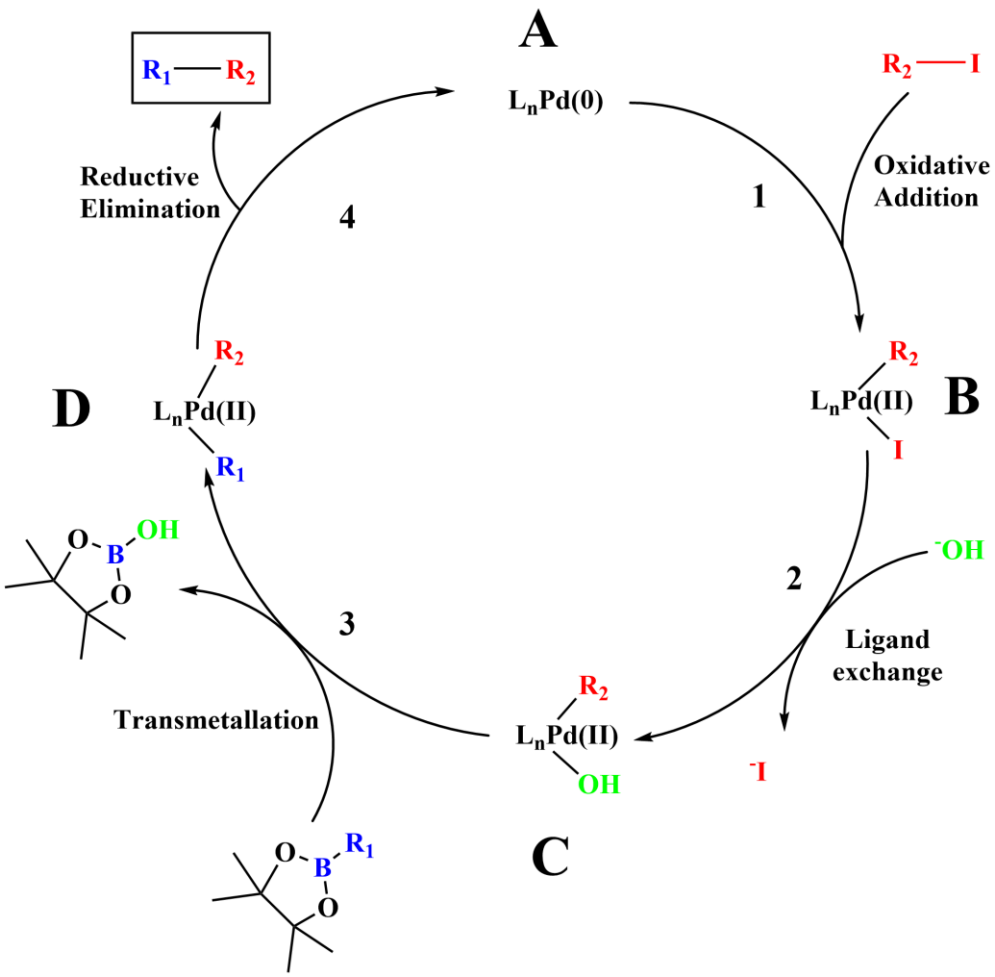

Scheme 10: An overview of the Suzuki-coupling mechanism catalyzed by Pd(0). 1) Oxidative addition of **Im-Pyr-Im**. 2) Halide exchanged for the base on the Pd(II). 3) Transmetallation of the R-group in **B.I** onto the Pd(II) catalyst. 4) Reductive elimination of **B.II**.

Similarly, to the Miyaura borylation in Subsection 3.3.1., every **B.I** molecule is susceptible to engaging in the catalyst cycle up to three times as it has two bromides and the boron ester, which most likely had a negative impact since **B.I** could engage in homo-coupling. Nonetheless, iodides are usually more reactive than bromides in Suzuki-Miyaura couplings, which may have counteracted the previously mentioned point as the only iodide is present on **Im-Pyr-Im** [39].

3.4. Methylation of Imidazoles Followed by Counterion Substitution

This reaction was done to convert the ligands **A.IV** and **B.II** (reactions **v** and **ix**) to pre-NHC ligands. The reaction conditions were the exact same and utilized iodomethane to convert the imidazole groups to imidazoliums. The reaction involved a nucleophilic attack (S_N2) from the imidazole on the methyl group, expelling the iodide in the process. The second step involved the swapping of the counterion ($2I^-$ from the solution) to PF_6^-, which accomplishes a variety of things: (1) an easy workup as the salt that is precipitated is water, making purification easy and efficient with high yields. (2) Prevents a mixture of multiple counterions in a batch, which would make molecular weight impossible to assess for future reactions and possibly make characterization and utilization give inconsistent results. (3) Makes the compound easier to dissolve in organic solvents. **A.V** and **B.III** were obtained with an average yield of 86 % and 93 % respectively.

3.5. Synthesis of Ligand C

Ligand C (**C.I**) was synthesized with the purpose of attempting a heteroleptic complex in combination with any successful homoleptically complexed ligand. It involved a one-step synthesis (Scheme 11), where the lone electron pair of the nitrogen in methylimidazole attacks the ortho carbons in the pyridine ring, eliminating the bromides in the process in a S_NAr reaction. The reaction is facilitated by the strong electron-withdrawing carboxyl group, which makes the pyridine ring more electron-deficient, but also by the pyridine-nitrogen's capability of stabilizing the incoming electron density from the methylimidazole. The bromides were later substituted with PF_6^- for the same reasons mentioned in Subsection 3.4..

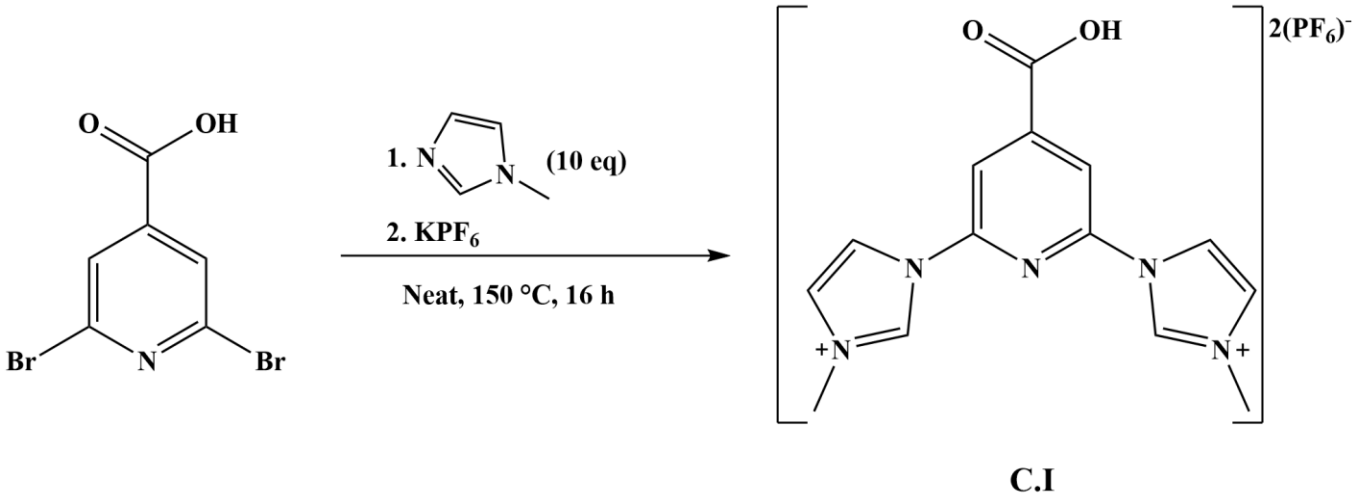

C.I

Scheme 11: The synthesis of **C.I** including counterion substitution with PF_6^-.

3.6. Fe(II)NHC Complexation

The complexation process introduced a base to form the carbenes on the carbons between the heteroatoms by deprotonating both imidazolium rings as depicted in Scheme 12. This was followed by the addition of the anhydrous Fe(II) source which would form a complex facilitated by the strong σ-donation by the carbenes onto the Fe(II) d-orbitals (as mentioned in Subsection 1.3.1.).

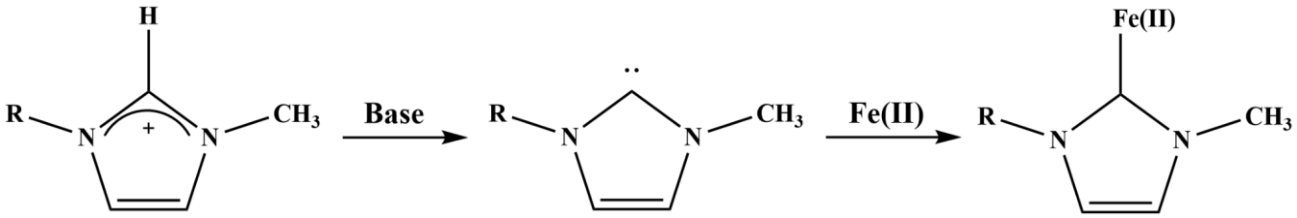

Scheme 12: The formation of the carbene and the complexation of the NHC to Fe(II).

3.6.1. Homoleptic Fe(II)NHC Complexation

Three homoleptic complexations were attempted with ligands **A.V**, **A.VI,** and **B.III**. **A.V** and **A.VI** were unsuccessful, most likely due to some sort of degradation of the ligands. The complexation conditions of **A.V** is illustrated in Scheme 13 and involved LDA (prepared *in situ*) as the base to prepare the NHC for the addition of $FeBr_2$ as the iron source. Theoretically, the LDA should do a lithium-hydrogen exchange with the very acidic hydrogen that is bonded to the carbon in between the two nitrogens in the imidazolium, which would form a highly polarized C-Li bond leading to a transmetallation (upon iron addition) where the carbon attacks the electron-deficient Fe(II) when it is added and forming a complex with it instead of the Li. The complexation attempt yielded two purple solids that could not be characterized. The ^{1}H NMR (Figure A12) of the crude showed a substantial amount of starting material (**A.V**), the persistent peak at ~9.5 ppm was the hydrogen that was supposed to engage in the lithium-hydrogen exchange and it was either not fully consumed or it may have been protonated back by a proton-source in the reaction (unlikely) or in the workup. Another notable remark is that the peak shifted slightly less at ~9.3 ppm is a new peak that could have appeared due to some sort of degradation of the ligand, leading to a slight shift in the spectra.

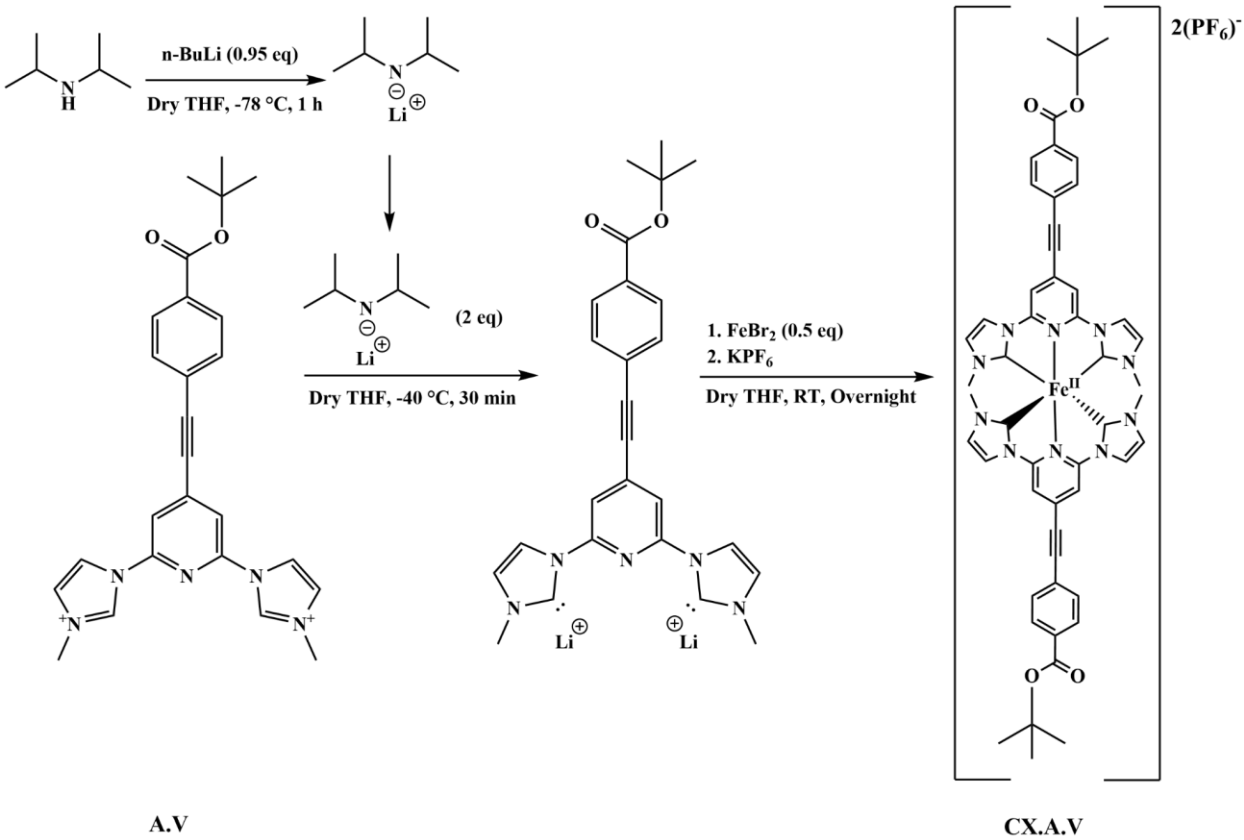

Scheme 13: The three-step reaction conditions of the attempt to complex **CX.A.V**. (1) synthesis of LDA. (2) Lithium-hydrogen exchange on both imidazolium. (3) The addition of Fe(II) and complexation followed by counterion substitution with PF_6^-.

Ligand **A.VI** was the deprotected analog of **A.V** (see Subsection 3.2.3.). The complexation of the **A.VI** was done to assess if the deprotected ligand could be complexed considering that the protecting group could have caused side-reaction or degradation of the **A.V** under basic conditions. It is hypothetically possible for the base to deprotonate one of the nine hydrogens on the *t*-butyl group of **A.V**. This would form a carboxylate on the ligand, but also a leaving isobutene. Alkenes and carbenes are known to react together to form cyclopropanes and this could have been the reason why the complexation of **A.V** didn't work [40], [41]. The formation of a carboxylate would also consume one equivalent of base, which would mean that the pre-NHCs wouldn't be fully deprotonated as it would leave 1.5 equivalent of base to deprotonate 2 equivalents of pre-NHCs.

The complexation of **A.VI** involved KO*t*-Bu as the base with one additional equivalent (3.5 total equivalence) to accommodate for the proton in the carboxyl group and $FeBr_2$ as the Fe(II) source (Scheme 14). The results in this attempt were very similar to the attempt above as the reaction gave a purple salt that could not be characterized after purification. Unlike the case with **A.V**, there was no sign of any starting material in this attempt, only a bulk of aromatic peaks (ppm > 6.5).

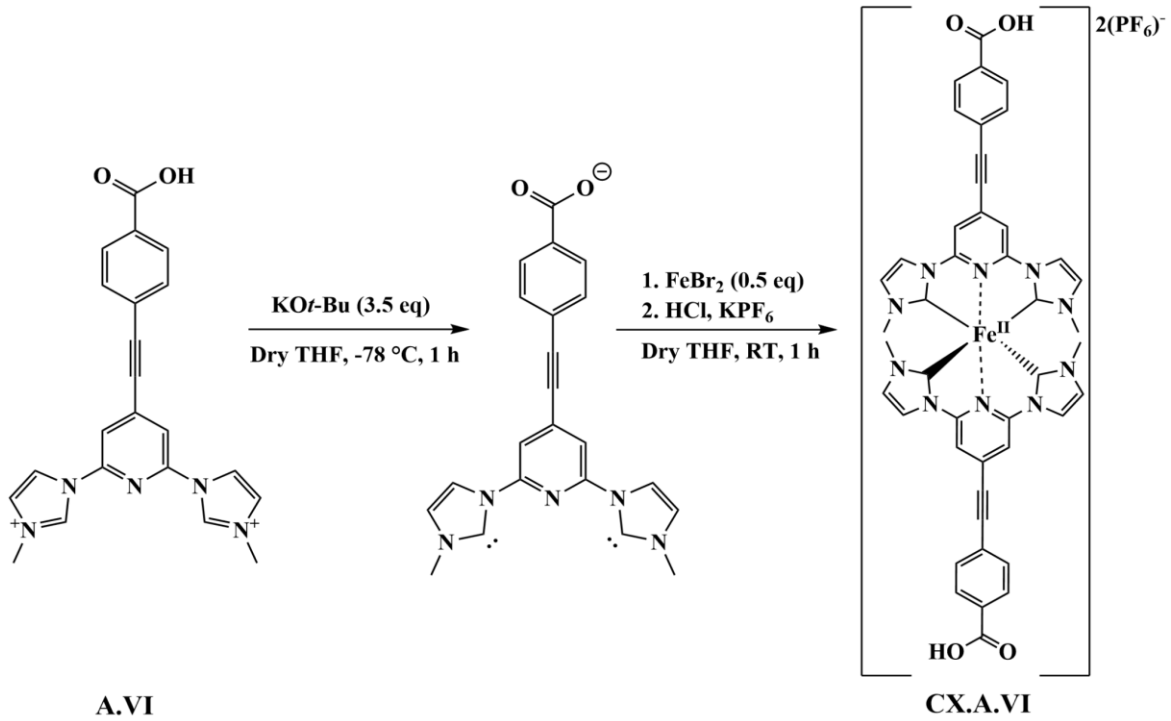

Scheme 14: The three-step conditions of the attempt to complex **CX.A.VI**.

The overview of the complexation of ligand **B.III** can be viewed in Scheme 15. It was done under the same overall conditions as the complexation of **A.VI**, but with a lower amount of base due to **B.III** lacking a carboxyl group. This reaction was done once and gave a successful yield of 30 %. The yield was relatively low, but could be improved by increasing the scale as this experiment was on the low end and any small errors or losses during the work-up could have greatly impacted the yield.

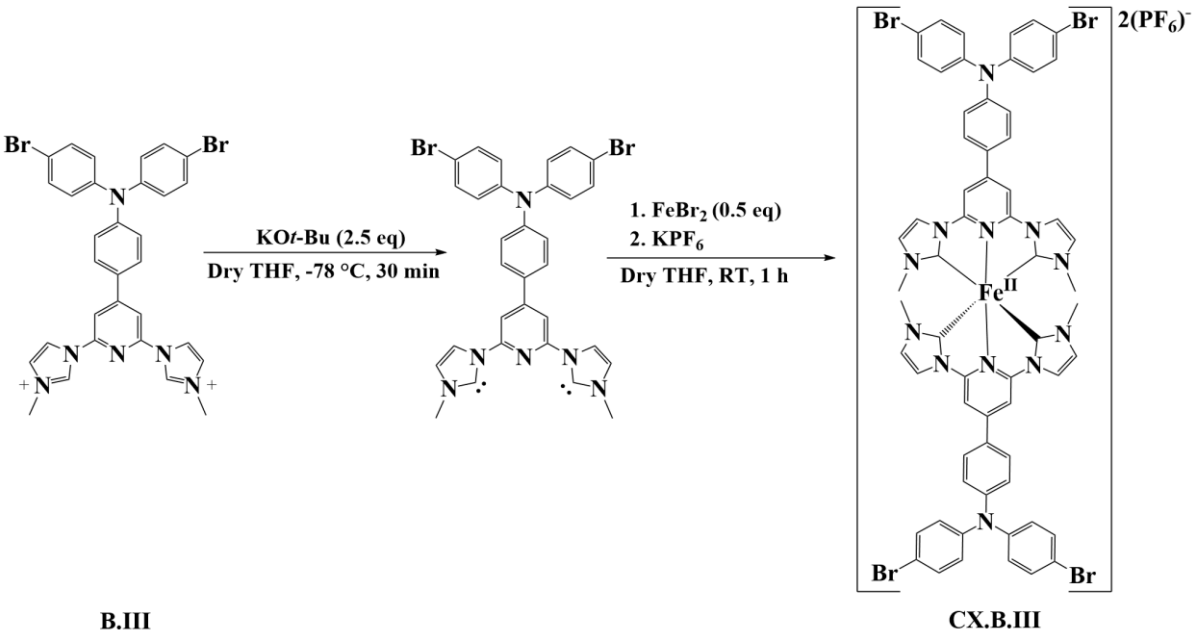

Scheme 15: The reaction conditions in the synthesis of **CX.B.III**.

3.6.2. Heteroleptic Fe(II)NHC Complexation

One heteroleptic complexation to Fe(II) was attempted with **B.III** and **C.I** (1:1 molar ratio) as the ligands and the conditions are available in Scheme 16. The complexation was successful as **CX.B.III.C.I** was isolated and the conditions were similar to that of the homoleptic complexation of **B.III** (Scheme 15) with the differences being DMF as the solvent at 0 °C (first step) and one additional equivalence of KO*t*-Bu (relative to **C.I**) to accommodate for the acidic proton in the carboxyl group of **C.I**. As expected, **CX.B.III** and **CX.C.I** (homoleptic complex of **C.I**) were also obtained and isolated from this reaction since the homoleptic complexation of each ligand is always inevitable. If the coordination rate of both ligands is equal, then the complexation would be distributed in an even fashion, giving 25 % of each homoleptic complex (50 % total) and 50 % of the heteroleptic complex (**CX.B.III.C.I**), meaning that the yield couldn't exceed 50 %. Regardless, a yield of 6 % was obtained which is far from ideal, but it could be improved by doing the reaction at a larger scale and perhaps with some optimization in the purification process. A significant amount of precipitate formed during the reaction and the compound could not be determined from the corresponding proton NMR due to having too many peaks, especially in the aromatic region. In hindsight, the precipitate could have contained a mix of the complexes and some additional product could possibly have been isolated from it, this was unfortunately not considered at the time, and this led to the precipitate being discarded.

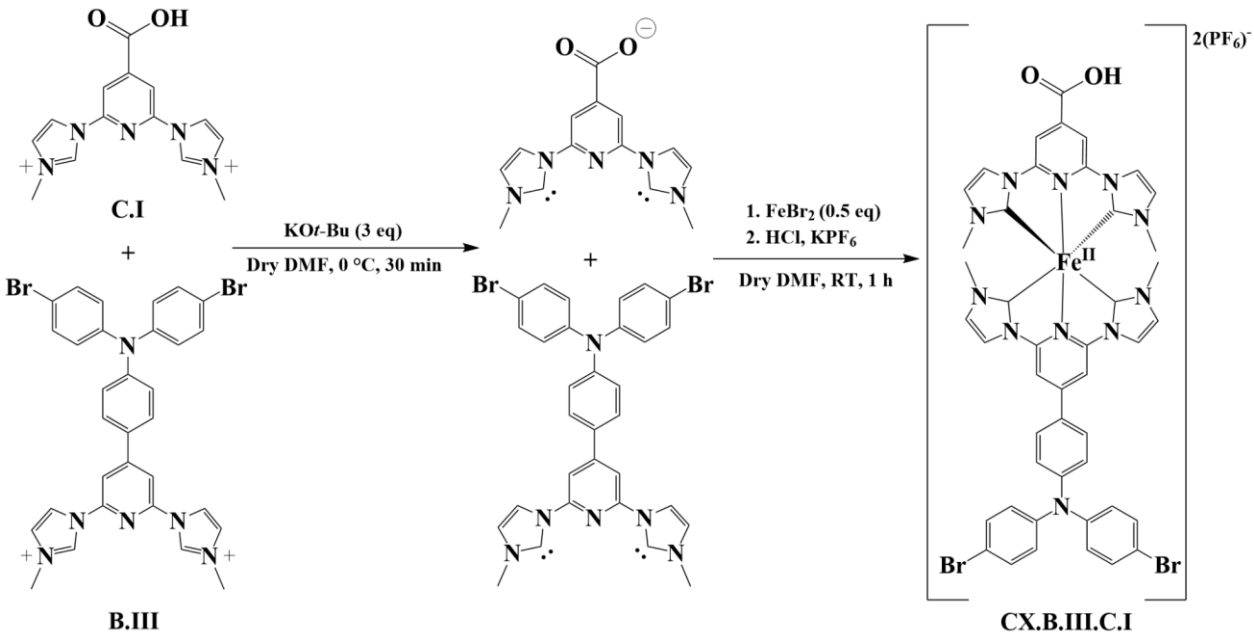

Scheme 16: The conditions of the heteroleptic complexation of **B.III** and **C.I** with Fe(II).

4. Conclusion and Future Prospects

Four NHC ligands, **A.V**, **A.VI**, **B.III**, and **C.I**, were successfully synthesized. The complexation of **A.V** and **A.VI** were unsuccessful, most likely due to the degradation of the ligands in the reaction. The novel ligand, **B.III**, was successfully complexed homoleptically and heteroleptically with **C.I** to Fe(II). **B.IV** and **B.V** were not synthesized due to a lack of time.

It is important to know why the complexations with **A.V** and **A.VI** and other ligands with acetylene groups are difficult to complex so that a solution can be strategized. One place to start is to find out in which step the complexation goes wrong and find a solution accordingly. Deuterated water could be used to quench the reaction after the addition of the base to form the NHCs. The NHCs should form a bond with the deuterated hydrogens if the deprotonation is working correctly. If the base is acting elsewhere, then we would be able to characterize the deuterated ligand and extract some valuable information.
As for ligand B, the bromides on both phenyls present an excellent opportunity for further syntheses to further alter the electronics of the ligand. One example would be to substitute the electron-withdrawing bromides with EDGs such as methoxy or anisole groups to get ligands **B.IV** and **B.V**, but other EDGs could also be considered.
Further optimization of the low-yielding boronated product (**B.I**) could be plausible with the solutions mentioned in Subsection 3.3.1., but could ultimately need a different work-up or purification method altogether to get moderate to high yields.

5. Experimental Section

5.1. Materials and Instruments

All the reagents and solvents that were not synthesized were available or purchased with 95 % purity or greater. The RT in the lab was 22 °C. All reaction vessels were pre-dried in an oven at 150 °C and pre-flushed with vacuum and nitrogen gas through a Schlenk line. Dry THF was distilled the same day. All other dry solvents were collected from a solvent dispenser or were commercially available and were further dried over molecular sieves with pore sizes of 3 Å diameter. SiO_2 (Silica) gel was used in both column chromatography (60 Å pores, 230-400 mesh, 60737) and coated TLC plates (60, F254) to monitor and purify the products in the ligand syntheses. Activated, neutral Al_2O_3 (alumina) was used in both column chromatography (60, F254) and Coated TLC plates (60, F254) to monitor and purify the complexes. NMR spectrums were recorded with a Bruker DRX spectrometer (400 MHz). The NMR spectrums were calibrated using the chemical shift (ppm) of the solvents (Chloroform-*d* (7.24 ppm), Acetonitrile-d_3 (1.94 ppm)). All solvents used in reactions and purification were removed using a rotary evaporator (Hei-VAP Core).

5.2. Method

2,6-Diimidazol-4-iodopyridine (Im-Pyr-Im)

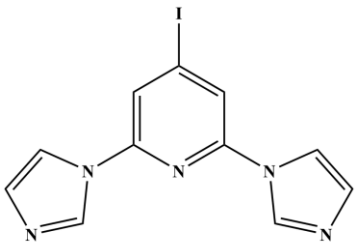

Chemical Formula: $C_{11}H_8IN_5$
Molecular Weight: 337.12 g/mol

A suspension of NaH (233 mg, 5.825 mmol, 60 wt % in mineral oil) was washed in *n*-hexane (4 × 15 mL) and to the residues was added dry DMF (35 mL). The mixture was cooled down to 0 °C and to it was added imidazole (355 mg, 5.221 mmol) and the resulting mixture was stirred for 1 h at 0 °C under nitrogen gas. The reaction was allowed to warm to RT and to it was added 2,6-difluoro-4-iodopyridine (500 mg, 2.075 mmol). The resulting solution was heated to 50 °C and stirred for 18 h under nitrogen gas. The resulting mixture was diluted with H_2O (130 mL) and was extracted with $CHCl_3$ (3 × 130 mL). The combined organic phases were consecutively washed with H_2O (130 mL) and brine (130 mL). The combined organic phases were evaporated *in vacuo* and the residue was consecutively washed with H_2O and Et_2O. Compound **Im-Pyr-Im** was obtained as an off-white solid (518 mg, 74%).
^{1}H NMR (400 MHz, Chloroform-*d*) δ 8.35 (t, *J* = 1.1 Hz, 2H), 7.64 (s, 2H), 7.62 (t, *J* = 1.4 Hz, 2H), 7.24 (dd, *J* = 1.5, 0.9 Hz, 2H).

5.2.1. Ligand A

tert-Butyl-4-iodo-benzoate (A.I)

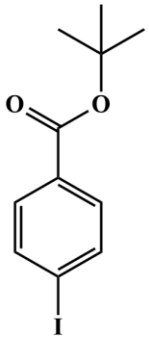

Chemical Formula: $C_{11}H_{13}IO_2$
Molecular Weight: 304.13 g/mol

To 4-iodobenzoic acid (500 mg, 2.02 mmol) was added $SOCl_2$ (2.6 mL, 5.302 mmol) and one drop of DMF. The resulting solution was refluxed for 30 minutes at 75 °C while stirring under nitrogen gas. The reaction was allowed to cool to RT and the remaining $SOCl_2$ was removed *in vacuo*. To the residues were dissolved in DCM (9 mL) and to the resulting solution was added KO*t*-Bu (250 mg, 2.24 mmol). The mixture was stirred for 18 h under nitrogen gas at RT. The resulting mixture was diluted with H_2O (25 mL) and the aqueous phase was extracted with DCM (3 × 20 mL). The combined organic phases were dried over $MgSO_4$, and evaporated *in vacuo*. To the product, diethyl ether (20 mL) was added. The mixture was filtered, and the filtrate was evaporated *in vacuo*. The starting material and compound **A.I** was acquired as orange/yellow crystalline solid.
^{1}H NMR (400 MHz, Chloroform-*d*) δ 7.79 – 7.74 (m, 2H), 7.71 – 7.66 (m, 2H), 1.58 (s, 9H).

tert-Butyl 4-((trimethylsilyl)ethynyl)benzoate (A.II)

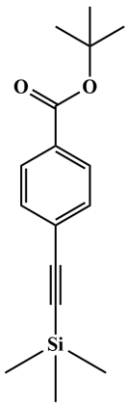

Chemical Formula: $C_{16}H_{22}O_2Si$
Molecular Weight: 274.44 g/mol

To a degassed suspension of **A.I** (454 mg, 1.495 mmol), $Pd(PPh_3)_2Cl_2$ (52.6 mg, 0.075 mmol) and, CuI (7.6 mg, 0.040 mmol) in anhydrous Et_3N (12 mL) was added ethynyltrimethylsilane (0.42 mL, 3.132 mmol). The reaction mixture was stirred at RT for 18 h under nitrogen. The resulting mixture was diluted with diethyl ether (20 mL) and vacuum filtered through pad of silica gel (3 × 3 cm). The filtrate was evaporated *in vacuo* and the product was purified by flash

chromatography on silica gel (3.5 × 15 cm, PE:EA (29:1)). Compound **A.II** was acquired as a yellow powder (296 mg, 72%).
^{1}H NMR (400 MHz, Chloroform-*d*) δ 7.91 (d, *J* = 8.4 Hz, 2H), 7.48 (d, *J* = 8.5 Hz, 2H), 1.59 (s, 9H), 0.26 (s, 9H).

tert-Butyl 4-ethynylbenzoate (A.III)

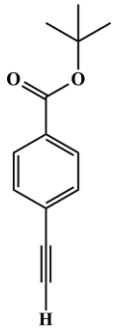

Chemical Formula: $C_{13}H_{14}O_2$
Molecular Weight: 202.25 g/mol

To a suspension of **A.II** (296 mg, 1.079 mmol) in DMF (5 mL) and H_2O (1.2 mL) was added KF (173 mg, 2.976 mmol). The solution was stirred for 40 min at RT. The solution was diluted with Et_2O (30 mL) and vacuum filtered through a pad of silica gel (3 × 3 cm). The filtrate was washed consecutively with H_2O (2 × 30 mL) and brine (2 × 30 mL), dried over $MgSO_4$ and evaporated *in vacuo*. The product was purified by sublimation at 80 ℃. Compound **A.III** was acquired as a white crystalline solid (128 mg, 59 %).
^{1}H NMR (400 MHz, Chloroform-*d*) δ 7.98 – 7.91 (m, 2H), 7.54 – 7.49 (m, 2H), 3.21 (s, 1H), 1.54 (s, 9H) ppm.

tert-Butyl 4-((di(imidazole-1-yl)pyridine-4-yl)ethynyl)benzoate (A.IV)

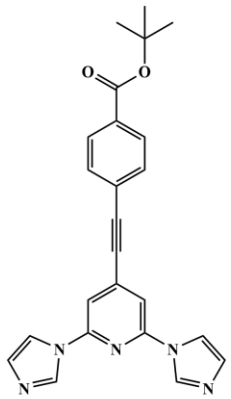

Chemical Formula: $C_{24}H_{21}N_5O_2$
Molecular Weight: 411.47

A solution of **A.III** (79 mg, 0.391 mmol) in dry DMF (6 mL) and a solution of **Im-Pyr-Im** (120 mg, 0.356 mmol), $Pd(PPh_3)_2Cl_2$ (29 mg, 0.041 mmol), CuI (9.0 mg, 0.047 mmol) in DMF (7 mL) and DIPA(0.9 mL) were degassed with argon for 20 minutes. To the **Im-Pyr-Im** solution was added the **A.III** solution slowly over 2 minutes. The resulting mixture was stirred at RT for 18 h under nitrogen gas. The resulting mixture was diluted with sat. NH_4Cl (20 mL) solution and

extracted with $CHCl_3$ (3 × 15 mL). The combined organic phases were washed with brine (35 mL), dried over $MgSO_4$, and evaporated *in vacuo*. The product was purified by flash chromatography on silica gel (3.5 × 15 cm, DCM:MeOH (24:1)). Compound **A.IV** was acquired as a off-white crystalline solid (118 mg, 81%).
^{1}H NMR (400 MHz, Acetonitrile-d_3) δ 8.47 (s, 2H), 8.07 – 8.00 (m, 2H), 7.86 (s, 2H), 7.74 – 7.68 (m, 2H), 7.65 (s, 2H), 7.16 (d, *J* = 1.4 Hz, 2H), 1.59 (s, 9H).

1,1'-(4-((4-(*tert*-Butoxycarbonyl)phenyl)ethynyl)pyridine-2,6-diyl)bis(3-methylimidazolium)Bis(hexafluorophosphate) (A.V)

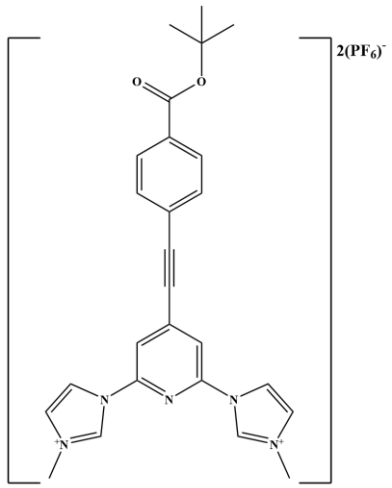

Chemical Formula: $C_{26}H_{27}N_5O_2P_2F_{12}$
Molecular Weight: 731.45 g/mol

To a solution of **A.IV** (50 mg, 0.112 mmol) in dry DMF (2.5 mL) was slowly added MeI (0.04 mL, 0.604 mmol) under nitrogen gas. The reaction mixture was heated to 130 °C and stirred for 1.5 h. The resulting mixture was allowed to cool to RT before being diluted with Et_2O (30 mL). The resulting precipitate was filtered off and dissolved in acidic MeOH solution (30 mL containing 10 drops of HCl (37%)). To the resulting solution was added KPF_6 (sat. aq., 40 mL) and the resulting precipitate was filtered, and the filter cake was washed with H_2O (50 mL) and Et_2O (25 mL) consecutively. The filter cake was filtered by dissolving it in CH_3CN and the solvent was evaporated *in vacuo*. Compound **A.V** was acquired as an off-white powder (70 mg, 86%).
^{1}H NMR (400 MHz, Acetonitrile-d_3) δ 9.51 (s, 2H), 8.18 (t, *J* = 2.0 Hz, 2H), 8.10 – 8.04 (m, 4H), 7.75 (d, *J* = 8.4 Hz, 2H), 7.64 (t, *J* = 1.9 Hz, 2H), 4.01 (s, 6H), 1.59 (s, 9H).

1,1'-(4-((4-Carboxyphenyl)ethynyl)pyridine-2,6-diyl)bis(3-methyl-1H-imidazol-3-ium)Bis(hexafluorophosphate) (A.VI)

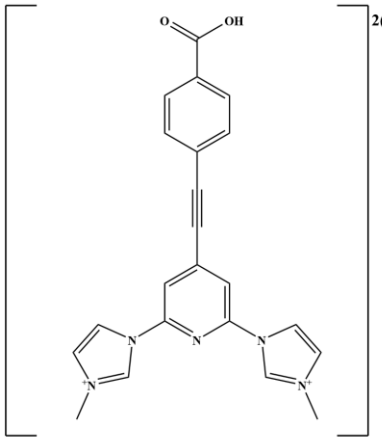

Chemical Formula: $C_{22}H_{19}N_5O_2P_2F_{12}$
Molecular Weight: 675.35 g/mol

To a solution of **A.V** (64 mg, 0.0948 mmol) in DCM (6.4 mL) was added TFA (3.2 mL, 4.08 mmol). The reaction solution was stirred at RT overnight. The resulting mixture was diluted with Et_2O (30 mL) and the resulting precipitate was filtered off and washed with Et_2O (25 mL). The filter cake was dissolved in acidic MeOH solution (25 mL containing 10 drops of HCl (37%)) and to the resulting solution was added KPF_6 (sat. aq., 25 mL). The resulting precipitate was filtered, and the filter cake was washed with H_2O and Et_2O consecutively. The filter cake was filtered by dissolving it in CH_3CN and the solvent was evaporated *in vacuo*. Compound **A.VI** was acquired as an off-white solid. (51 mg, 86 %)
^{1}H NMR (400 MHz, Acetonitrile-d_3) δ 9.86 (s, 2H), 8.17 (s, 2H), 8.10 (d, J = 8.2 Hz, 2H), 8.07 (s, 2H), 7.77 (d, J = 8.4 Hz, 2H), 7.62 (s, 2H), 4.03 (s, 6H).

5.2.2. Ligand B

4-Bromo-N-(4-bromophenyl)-N-(4-(4,4,5,5-tetramethyl-1,3,2-dioxaborolane-2-yl)phenyl)aniline (**B.I**)

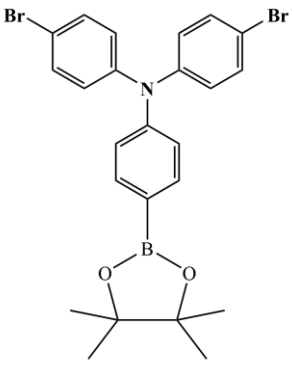

Chemical Formula: $C_{24}H_{24}BBr_2NO_2$
Molecular Weight: 529.08 g/mol

A suspension of Tris(4-bromophenyl)amine (500 mg, 1.037 mmol), Bis(pinacolato)diboron (290 mg, 1.141 mmol) and KOAc (305 mg, 3.112 mmol) were dissolved in dry 1,4-dioxane and the mixture was purged with argon for 15 min. To the resulting solution was added $Pd(dppf)Cl_2$ (38 mg, 0.05187 mmol) and the reaction was stirred at reflux for 24 h under argon gas. The resulting mixture was quenched with brine (100 mL) and extracted with DCM (3 × 100 mL). The combined organic phases were dried over Na_2SO_4, and the solvents were removed *in vacuo*. The product was purified by flash chromatography in silica gel (3.5 × 15 cm, PE:EA (29:1)). **B.I** was acquired as a off-white solid. (194 mg, 35%)

^{1}H NMR (400 MHz, Chloroform-*d*) δ 7.73 – 7.62 (m, 2H), 7.40 – 7.29 (m, 4H), 7.07 – 6.99 (m, 2H), 6.99 – 6.90 (m, 4H), 1.34 (s, 12H).

4-Bromo-N-(4-bromophenyl)-N-(4-(2,6-di(1H-imidazol-1-yl)pyridin-4-yl) phenyl)aniline (**B.II**)

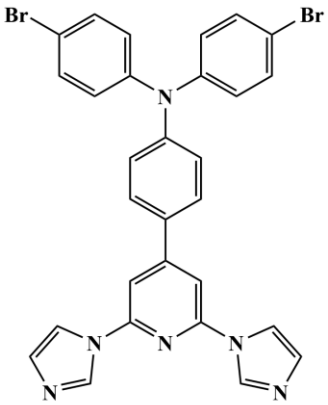

Chemical Formula: $C_{29}H_{20}Br_2N_6$
Molecular Weight: 612.33 g/mol

A suspension of **B.I** (97 mg, 0.1828 mmol), **Im-Pyr-Im** (54 mg, 0.1589 mmol) and K_2CO_3 (63 mg, 0.457 mmol) was dissolved in a solution of toluene (10 mL), EtOH (2 mL) and H_2O (0.4 mL) and the resulting mixture was purged with argon for 15 min. To the mixture was added $Pd(PPh_3)_4$ (9.2 mg, 0.009139 mmol) and the resulting mixture was stirred at reflux for 18 h under argon gas. The resulting mixture was quenched with H_2O (25 mL) and extracted with EA (3 × 25 mL). The combined organic phases were dried over Na_2SO_4, and the solvents were removed *in vacuo*. The product was purified by flash chromatography on silica gel (3.5 × 15 cm, DCM:Acetone:MeOH (90:6:4)). Compound **B.II** was acquired as a white powder. (78 mg, 80 %)

^{1}H NMR (400 MHz, Chloroform-*d*) δ 8.43 (s, 2H), 7.72 (t, *J* = 1.4 Hz, 2H), 7.57 (d, *J* = 8.7 Hz, 2H), 7.47 – 7.40 (m, 4H), 7.39 (s, 2H), 7.25 (t, *J* = 1.2 Hz, 2H), 7.20 – 7.13 (m, 2H), 7.04 – 7.00 (m, 4H).

1,1'-(4-(4-(Bis(4-bromophenyl)amino)phenyl)pyridine-2,6-diyl)bis(3-methyl-1H-imidazol-3-ium)bis(hexafluorophosphate) (**B.III**)

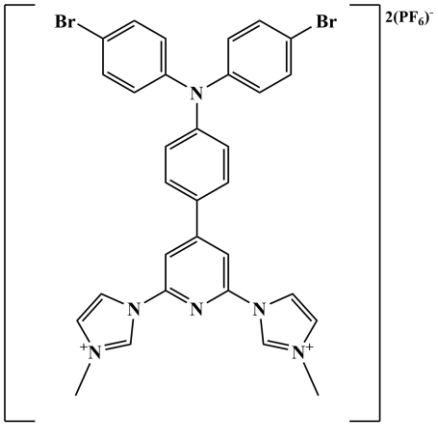

Chemical Formula: $C_{31}H_{26}Br_2N_6P_2F_{12}$
Molecular Weight: 932.31 g/mol

To a solution of **B.II** (70 mg, 0.1143 mmol) in dry DMF (3 mL) was slowly added MeI (0.04 mL, 0.64184 mmol) under nitrogen gas. The resulting mixture was sealed and stirred at 130 °C for 1 h. The resulting mixture was allowed to cool to RT before being diluted with Et_2O (50 mL). The resulting precipitate was filtered off and dissolved in acidic MeOH solution (50 mL containing 30 drops of HCl (37 %)) and to the resulting solution was added KPF_6 (sat. aq., 40 mL). The resulting precipitate was filtered, and the filter cake was washed with H_2O and Et_2O consecutively. The filter cake was filtered by dissolving it in CH_3CN and the solvent was evaporated *in vacuo*. **B.III** was acquired as a yellow crystalline solid (110 mg, 93 %) ^{1}H NMR (400 MHz, Acetonitrile-d_3) δ 9.83 (s, 2H), 8.26 (t, *J* = 2.0 Hz, 2H), 8.08 (s, 2H), 7.89 (d, *J* = 8.8 Hz, 2H), 7.61 (t, *J* = 1.9 Hz, 2H), 7.54 – 7.50 (m, 4H), 7.20 (d, *J* = 8.8 Hz, 2H), 7.11 – 7.05 (m, 4H), 4.02 (s, 6H).

5.2.3. Ligand C

1,1'-(4-Carboxypyridine-2,6-diyl)bis(3-methyl-1H-imidazol-3-ium) Bis(hexafluorophosphate) (C.I)

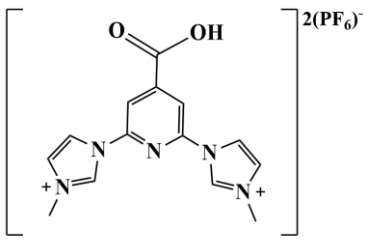

Chemical Formula: $C_{14}H_{15}N_5O_2P_2F_{12}$
Molecular Weight: 575.23 g/mol

A mixture of 2,6-dibromoisonicotinic acid (1 g, 3.56 mmol) and methylimidazole (3 mL, 37.6 mmol) under argon gas was sealed and the reaction was stirred at 150 °C for 20 h. The resulting mixture was allowed to reach RT before being diluted with Et_2O (40 mL) . The resulting mixture was stirred for 30 min. The solvents were decanted, and the residual solids were dissolved in a HCl solution (20 mL H_2O containing 20 drops HCl (37%)). To the resulting solution was added KPF_6 solution (sat. aq., 40 mL) and the resulting precipitate was filtered, and the filter cake was washed with water and Et_2O consecutively. Compound **C.I** was acquired as a gray solid (1.31 g, 64%).

^{1}H NMR (400 MHz, Acetonitrile-d_3) δ 10.56 (s, 2H), 8.74 (s, 2H), 8.34 (t, J = 1.9 Hz, 2H), 7.58 (t, J = 1.9 Hz, 2H), 4.08 (s, 6H).

5.2.4. Complexation

Bis(1,1'-(4-(4-(bis(4-bromophenyl)amino)phenyl)pyridine-2,6-diyl)bis(3-methyl-1H-imidazol-3-ium-2-ide))iron(II)bis(hexafluorophosphate) (**CX.B.III**)

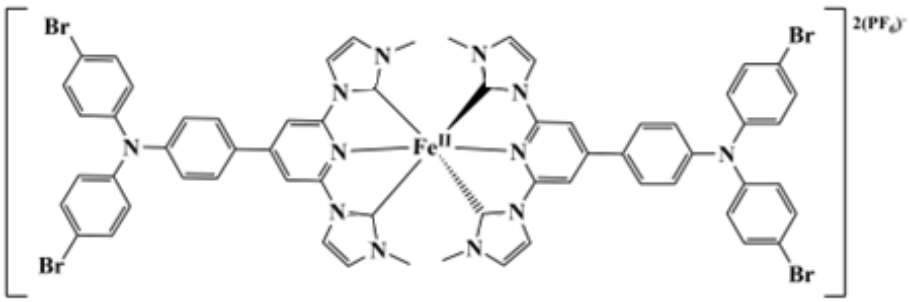

Chemical Formula: $C_{62}H_{48}Br_4FeN_{12}P_2F_{12}$
Molecular Weight: 1626.51 g/mol

A suspension of **B.III** (56 mg, 0.0607 mmol) was put under vacuum at 60 °C for 72 h to dry. To the suspension was added dry THF (5 mL) under nitrogen gas. The resulting mixture was cooled to -78 °C and to it was added a dry THF solution of KO*t*-Bu (0.15 mL, 0.15 mm, 1 M). The resulting mixture was stirred at -78 °C for 30 min. A solution of anhydrous $FeBr_2$ (8 mg, 0.0371 mmol) in dry THF (2 mL) was added and the resulting mixture was allowed to reach RT and was stirred for 1 h. The solvents were removed *in vacuo* and the residues were dissolved in acidic MeOH solution (30 mL containing 8 drops HCl (37 %)) followed by the addition of KPF_6 solution (sat. aq., 20 mL). The resulting precipitate was filtered, and the filter cake was washed with H_2O and Et_2O consecutively. The filter cake was filtered by dissolving it in CH_3CN and the solvent was evaporated *in vacuo*. The product was purified by flash chromatography on alumina gel (3.5 × 12 cm, CH_3CN:H_2O (95:5)). Compound **CX.B.III** was acquired as an orange crystalline solid. (31 mg, 30 %)

^{1}H NMR (400 MHz, Acetonitrile-d_3) δ 8.15 (d, J = 2.2 Hz, 2H), 8.08 (s, 2H), 8.02 (d, J = 8.7 Hz, 2H), 7.58 – 7.51 (m, 4H), 7.28 (d, J = 8.7 Hz, 2H), 7.16 – 7.08 (m, 4H), 7.04 (d, J = 2.1 Hz, 2H), 2.61 (s, 6H).

1,1'-(4-Carboxypyridine-2,6-diyl)bis(3-methyl-1H-imidazol-3-ium-2-ide)(1,1'-(4-(4-(bis(4-bromophenyl)amino)phenyl)pyridine-2,6-diyl)bis(3-methyl-1H-imidazol-3-ium-2-ide))iron(II)Bis(hexafluorophosphate) (**CX.B.III.C.I)**

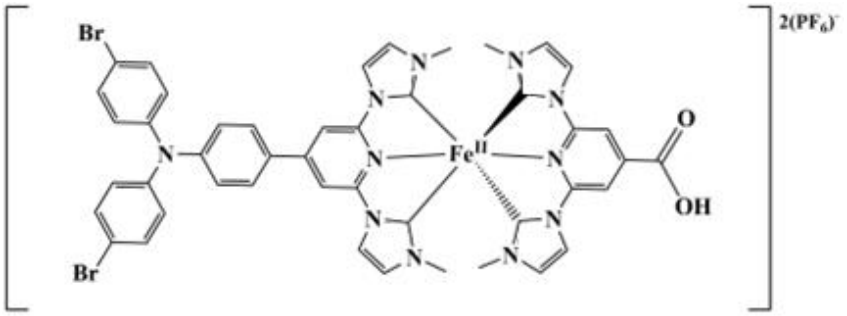

Chemical Formula: $C_{45}H_{37}Br_2FeN_{11}O_2P_2F_{12}$
Molecular Weight: 1269.43 g/mol

A suspension of **B.III** (47 mg, 0.0504 mmol) and **C.I** (29 mg, 0.0504 mmol) was put under vacuum at 60 °C for 72 h to dry. To the suspension was added dry and degassed DMF (4 mL) under nitrogen gas. The mixture was cooled to 0 °C and to it was added a dry THF solution of KO*t*-Bu (0.30 mL, 0.30 mm, 1 M) and the mixture was stirred at 0 °C for 30 min under nitrogen gas. A solution of anhydrous $FeBr_2$ (8 mg, 0.0371 mmol) in dry DMF (5 mL) and the resulting mixture was allowed to reach RT and was stirred for 1 h. The mixture was diluted with EA (25 mL) and H_2O (25 mL) and HCl (1 mL (37 %)). The organic phase was extracted with EA (25 mL × 3). The combined organic phases were dried over Na_2SO_4 and evaporated *in vacuo*. The product was purified by flash chromatography on alumina gel (3.5 × 12 cm, CH_3CN:H_2O ((90:10), (80:20), (75:25)). The solvents in the collected fractions were removed *in vacuo* and the product was dissolved in HCl solution (10 mL H_2O containing 20 drops HCl (37 %)) followed by the addition of KPF_6 until red precipitate formed. The resulting precipitate was filtered, and the filter cake was washed with H_2O and Et_2O consecutively. The filter cake was filtered by dissolving it in CH_3CN and the solvent was evaporated *in vacuo*. Compound **CX.B.III.C** was acquired as a red/orange crystalline solid. (4 mg, 6 %)

^{1}H NMR (400 MHz, Acetonitrile-d_3) δ 8.31 (s, 2H), 8.17 (d, J = 2.2 Hz, 2H), 8.10 (d, J = 2.2 Hz, 2H), 8.05 (s, 2H), 8.01 – 7.95 (m, 2H), 7.55 – 7.48 (m, 4H), 7.28 – 7.23 (m, 2H), 7.12 – 7.06 (m, 4H), 7.02 (d, J = 2.2 Hz, 2H), 7.00 (d, J = 2.2 Hz, 2H), 2.60 (s, 6H), 2.49 (s, 6H).

6. Reference List

[1] Exxonmobile, 'Energy demand: three drivers', Energy and innovation, outlook for energy, 2022, <https://corporate.exxonmobil.com/energy-and-innovation/outlook-for-energy/energy-demand>

[2] Stanford university, 'When Fossil Fuels Run Out, What Then?', 2019, <https://mahb.stanford.edu/library-item/fossil-fuels-run/#disqus_thread>

[3] Y. Liu, "A genome and gene catalog of glacier microbiomes", *Nature Biotechnology*, vol. 40, no. 9, pp. 1341–1348, 2022, doi: https://doi.org/10.1038/s41587-022-01367-2.

[4] United States Environmental Protection Agency, 'Climate Change Indicators: Weather and Climate', 2022, <https://www.epa.gov/climate-indicators/weather-climate#:~:text=Rising%20global%20average%20temperature%20is,with%20human%2Dinduced%20climate%20change>

[5] The Ocean Foundation, 'Ocean and Climate Change', 2023, <https://oceanfdn.org/ocean-and-climate-change/>

[6] A. Hagfeldt, G. Boschloo, L. Sun, L. Klooand H. Pettersson, "Dye-Sensitized Solar Cells", *Chemical Reviews*, vol. 110, no. 11, pp. 6595–6663, 2010, doi: https://doi.org/10.1021/cr900356p.

[7] B. O'Regan and M. Grätzel, "A low-cost, high-efficiency solar cell based on dye-sensitized colloidal TiO2 films", *Nature*, vol. 353, no. 6346, pp. 737–740, 1991, doi: https://doi.org/10.1038/353737a0.

[8] A. B. Muñoz-García, "Dye-sensitized solar cells strike back", *Chem. Soc. Rev.*, vol. 50, no. 22, pp. 12450–12550, 2021, doi: http://doi.org/10.1039/d0cs01336f

[9] Y. Wu, W.-H. Zhu, S. M. Zakeeruddinand M. Grätzel, "Insight into D–A−π–A Structured Sensitizers: A Promising Route to Highly Efficient and Stable Dye-Sensitized Solar Cells", *ACS Applied Materials & Interfaces*, vol. 7, no. 18, pp. 9307–9318, 2015, doi: http://doi.org/10.1021/acsami.5b02475

[10] N. Robertson, "Optimizing Dyes for Dye-Sensitized Solar Cells", *Angewandte Chemie International Edition*, vol. 45, no. 15, pp. 2338–2345, 2006, doi: http://doi.org/10.1002/anie.200503083

[11] A. S. Polo, M. K. Itokazu, N. Y. M. Iha, "Metal complex sensitizers in dye-sensitized solar cells", *Coordination Chemistry Review*s, V. 248, no. 13–14, pp. 1343-1361, ISSN 0010-8545, 2004, doi: https://doi.org/10.1016/j.ccr.2004.04.013.

[12] Y. Liu, P. Persson, V. Sundström and K. Wärnmark, "Fe N-Heterocyclic Carbene Complexes as Promising Photosensitizers", *Accounts of Chemical Research*, vol. 49, no. 8, pp. 1477–1485, 2016, doi: https://doi.org/10.1021/acs.accounts.6b00186.

[13] S. Malladi, S. Yarasiand G. N. Sastry, "Exploring the potential of iron to replace ruthenium in photosensitizers: a computational study", *Journal of Molecular Modeling*, vol. 24, no. 12, 2018, doi: https://doi.org/10.1007/s00894-018-3870-x

[14] S. Kaufhold and K. Wärnmark, "Design and Synthesis of Photoactive Iron N-Heterocyclic Carbene Complexes", *Catalysts*, vol. 10, no. 1, p. 132, 2020, doi: http://doi.org/10.3390/catal10010132

[15] J. Clayden, N. Greeves, S. Warren, "*Organic Chemistry*", 2nd ed., New York, University of Oxford Press, pp. 1004-1007, 2012.

[16] C. E. Housecroft, A. G. sharpe, "Inorganic Chemistry", 4th ed., Harlow England: Pearson, pp. 665-671, 2012.

[17] Y. Liu, "Towards longer-lived metal-to-ligand charge transfer states of iron(ii) complexes: an N-heterocyclic carbene approach", *Chem. Commun.*, vol. 49, no. 57, p. 6412, 2013, doi: http://doi.org/10.1039/c3cc43833c

[18] L. Mercs and M. Albrecht, "Beyond catalysis: N-heterocyclic carbene complexes as components for medicinal, luminescent, and functional materials applications", *Chem. Soc. Rev.*, vol. 39, no. 6, p. 1903, 2010, doi: http://doi.org/10.1039/b902238b.

[19] M. Darari, "Iron(ii) complexes with diazinyl-NHC ligands: impact of π-deficiency of the azine core on photophysical properties", *Dalton Trans.*, vol. 48, no. 29, pp. 10915–10926, 2019, doi: http://doi.org/10.1039/c9dt01731c.

[20] M. Pastore, "Interfacial charge separation and photovoltaic efficiency in Fe(ii)–carbene sensitized solar cells", *Phys. Chem. Chem. Phys.*, vol. 18, no. 40, pp. 28069–28081, 2016, doi: http://doi.org/10.1039/c6cp05535d.

[21] M. Karpacheva, C. E. Housecroftand E. C. Constable, "Electrolyte tuning in dye-sensitized solar cells with N-heterocyclic carbene (NHC) iron(II) sensitizers", *Beilstein Journal of Nanotechnology*, vol. 9, pp. 3069–3078, 2018, doi: http://doi.org/10.3762/bjnano.9.285.

[22] L. Lindh, "Dye-sensitized solar cells based on Fe N-heterocyclic carbene photosensitizers with improved rod-like push-pull functionality", *Chemical Science*, vol. 12, no. 48, pp. 16035–16053, 2021, doi: https://doi.org/10.1039/d1sc02963k.

[23] A. Reddy Marri, "Record power conversion efficiencies for iron(ii)-NHC-sensitized DSSCs from rational molecular engineering and electrolyte optimization", *Journal of Materials Chemistry A*, vol. 9, no. 6, pp. 3540–3554, 2021, doi: http://doi.org/10.1039/d0ta10841c

[24] K. Oum, "Electron and hole transfer dynamics of a triarylamine-based dye with peripheral hole acceptors on TiO2 in the absence and presence of solvent", *Physical Chemistry Chemical Physics*, vol. 16, no. 17, p. 8019, 2014, doi: https://doi.org/10.1039/c3cp55298e.

[25] Y. Hao, "Peripheral Hole Acceptor Moieties on an Organic Dye Improve Dye-Sensitized Solar Cell Performance", *Advanced Science*, vol. 2, no. 11, p. 1500174, 2015, doi: https://doi.org/10.1002/advs.201500174.

[26] J. Clayden, N. Greeves, S. Warren, "*Organic Chemistry*", 2nd ed., New York, University of Oxford Press, p. 741, 2012.

[27] J. Clayden, N. Greeves, S. Warren, "*Organic Chemistry*", 2nd ed., New York, University of Oxford Press, pp. 214-215, 733-735, 2012.

[28] R. Chinchilla and C. Nájera, "Recent advances in Sonogashira reactions", *Chemical Society Reviews*, vol. 40, no. 10, p. 5084, 2011, doi: http://doi.org/10.1039/c1cs15071e

[29] J. Clayden, N. Greeves, S. Warren, "*Organic Chemistry*", 2nd ed., New York, University of Oxford Press, pp. 1084-1090, 2012.

[30] A.Elangovan, Y. H. Wang, T. I. Ho, "Sonogashira Coupling Reaction with Diminished Homocoupling", *Org. Lett*, 5, pp. 1841−1844, 2003, doi: https://doi.org/10.1021/ol034320.

[31] J. Clayden, N. Greeves, S. Warren, "*Organic Chemistry*", 2nd ed., New York, University of Oxford Press, pp. 671-672, 2012.

[32] Larson GL. Some Aspects of the Chemistry of Alkynylsilanes. *Synthesis (Stuttg)*, 50(13):2433–62, 2018, doi: http://doi.org/10.1055/s-0036-1591979

[33] J. Clayden, N. Greeves, S. Warren, "*Organic Chemistry*", 2nd ed., New York, University of Oxford Press, pp. 209, 2012.

[34] G. A. Molander, S. L. J. Trice, S. M. Kennedy, S. D. Dreherand M. T. Tudge, "Scope of the Palladium-Catalyzed Aryl Borylation Utilizing Bis-Boronic Acid", *Journal of the American Chemical Society*, vol. 134, no. 28, pp. 11667–11673, 2012, doi: http://doi.org/10.1021/ja303181m

[35] S. Barroso, "Improvement in the Palladium-Catalyzed Miyaura Borylation Reaction by Optimization of the Base: Scope and Mechanistic Study", *The Journal of Organic Chemistry*, vol. 86, no. 1, pp. 103–109, 2021, doi: http://doi.org/10.1021/acs.joc.0c01758

[36] Mrinmoy Kumar Chini, Rajashree Y. Mahale, Shyambo Chatterjee, "Effect of heterocycles on field-effect transistor performances of donor-acceptor-donor type small molecules", *Chemical Physics Letters*, vol. 661, pp 107-113, ISSN 0009-2614, 2016, doi: https://doi.org/10.1016/j.cplett.2016.08.073

[37] E. K. Reeves, E. D. Entzand S. R. Neufeldt, "Chemodivergence between Electrophiles in Cross-Coupling Reactions", *Chemistry – A European Journal*, vol. 27, no. 20, pp. 6161–6177, 2021, doi: https://doi.org/10.1002/chem.202004437

[38] N. Oka, T. Yamada, H. Sajiki, S. Akaiand T. Ikawa, "Aryl Boronic Esters Are Stable on Silica Gel and Reactive under Suzuki–Miyaura Coupling Conditions", *Organic Letters*, vol. 24, no. 19, pp. 3510–3514, 2022, doi: http://doi.org/10.1021/acs.orglett.2c01174

[39] A. F. Littke, C. Daiand G. C. Fu, "Versatile Catalysts for the Suzuki Cross-Coupling of Arylboronic Acids with Aryl and Vinyl Halides and Triflates under Mild Conditions", *Journal of the American Chemical Society*, vol. 122, no. 17, pp. 4020–4028, 2000, doi: http://doi.org/10.1021/ja0002058

[40] J. Clayden, N. Greeves, S. Warren, "*Organic Chemistry*", 2nd ed., New York, *University of Oxford Press*, pp. 1013-1016, 2012.

[41] H. S. Yang, L. Macha, H.-J. Haand J. W. Yang, "Functionalisation of esters via 1,3-chelation using NaOtBu: mechanistic investigations and synthetic applications", *Organic Chemistry Frontiers*, vol. 8, no. 1, pp. 53–60, 2021, doi: http://doi.org/10.1039/d0qo01135e

7. Appendix

7.1. ^{1}H NMR

All relevant proton NMRs are available in this section. The protons have been linked with a number to their corresponding peak with a blue number. Some protons in the imidazolyl and methylimidazoliumyl groups have been colored red as these protons couldn't be linked to a specific peak due to these protons being indistinguishable from each other. Indistinguishable peaks have thus been labelled with a red colored X in the spectrums to highlight that they belong to one of the red colored protons.

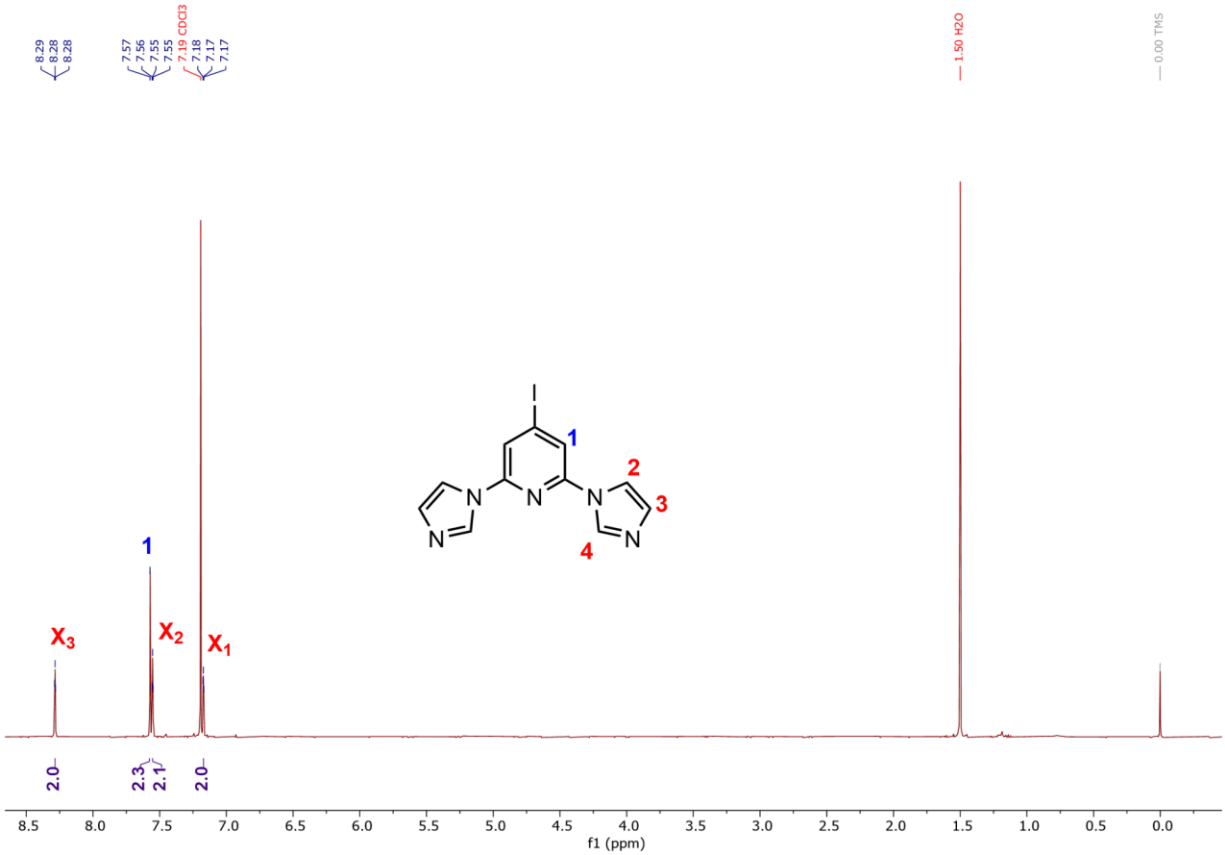

Figure A1: Proton NMR spectra of **Im-Pyr-Im.** Protons 2,3 and 4 are indistinguishable in the spectra and they were thus not assigned to any specific peak, but they belong to one of the X peaks.

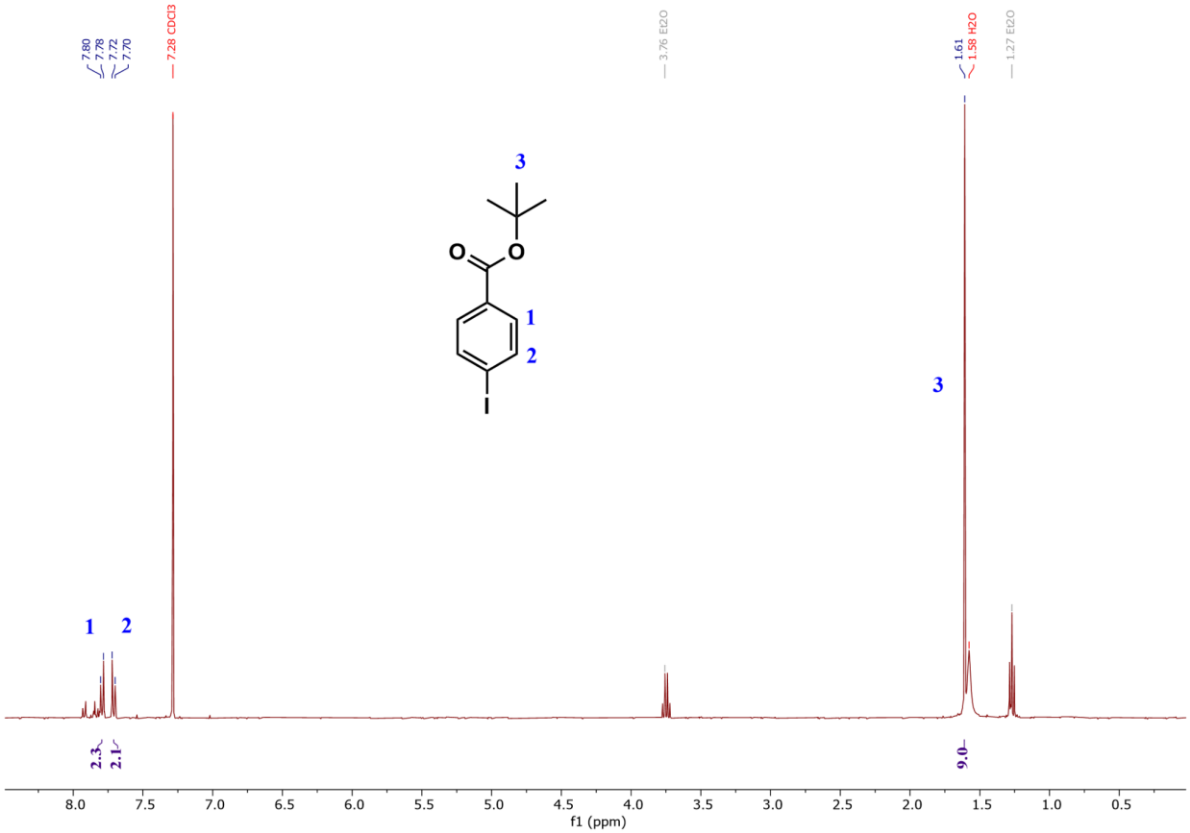

Figure A2: Proton NMR spectra of **A.I**, the numbered protons correspond to their respective peaks.

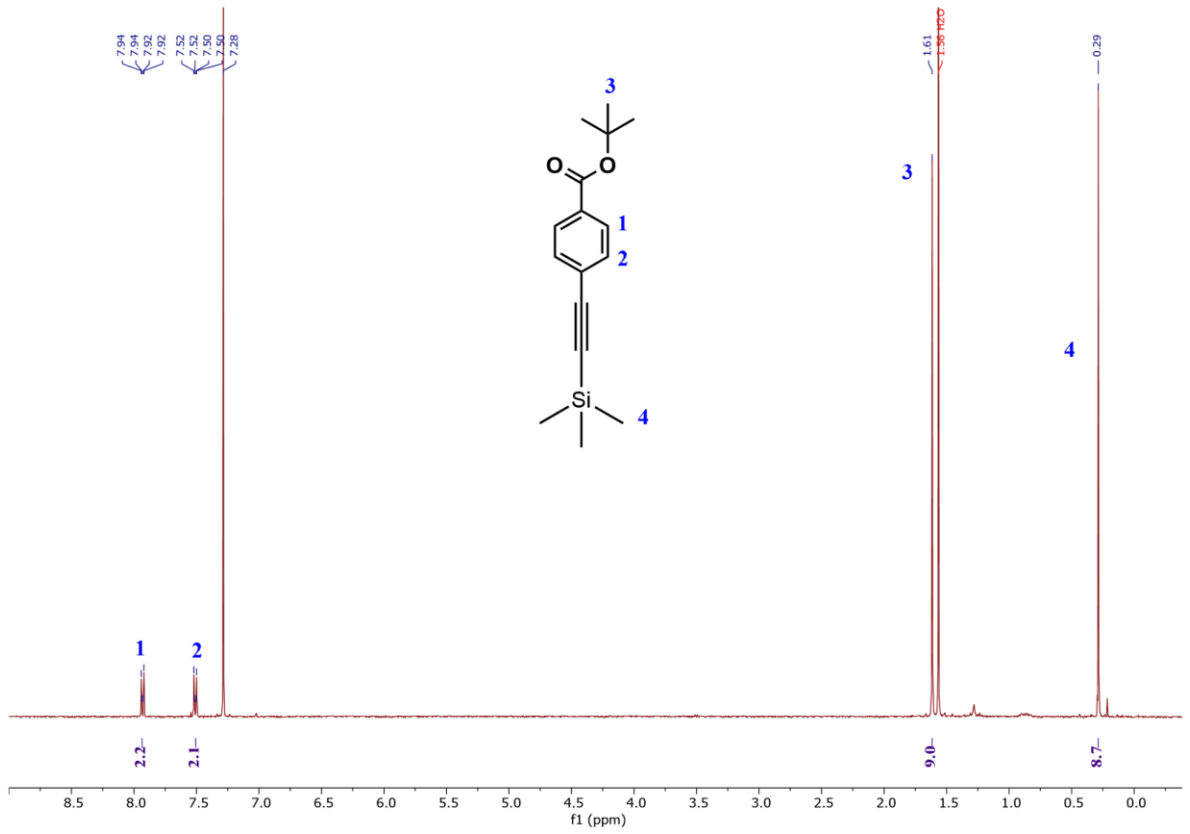

Figure A3: Proton NMR of **A.II**, the numbered protons correspond to their respective peaks.

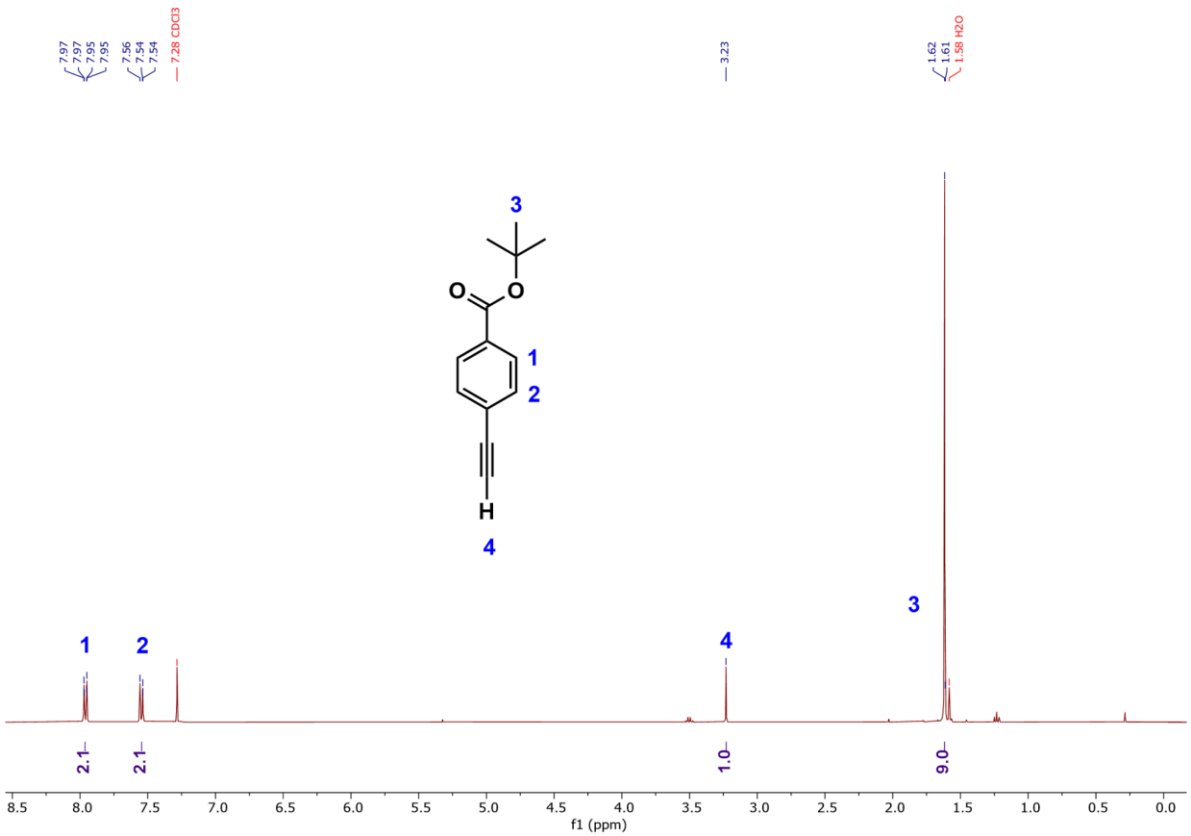

Figure A4: Proton NMR of **A.III**, the numbered protons correspond to their respective peaks.

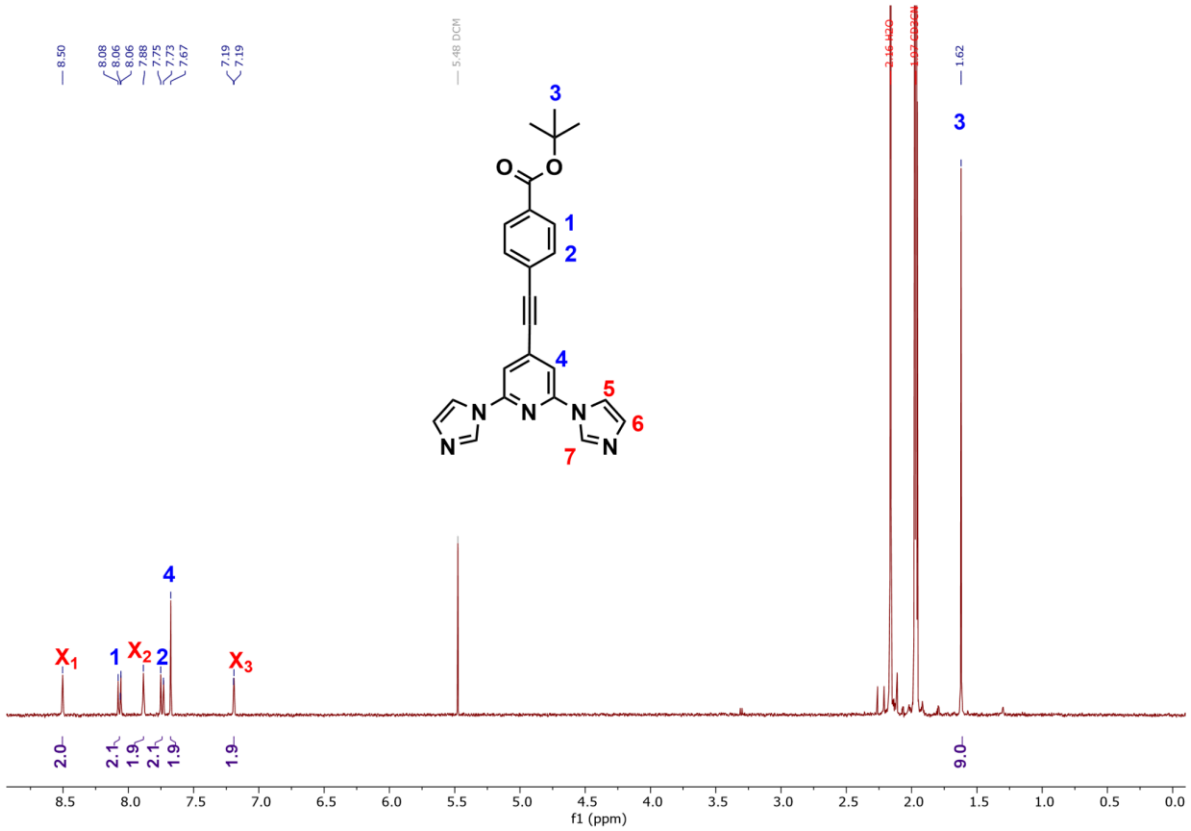

Figure A5: Proton NMR spectra of **A.IV**. Protons 5,6 and 7 are indistinguishable in the spectra and they were thus not assigned to any specific peak, but they belong to one of the X peaks.

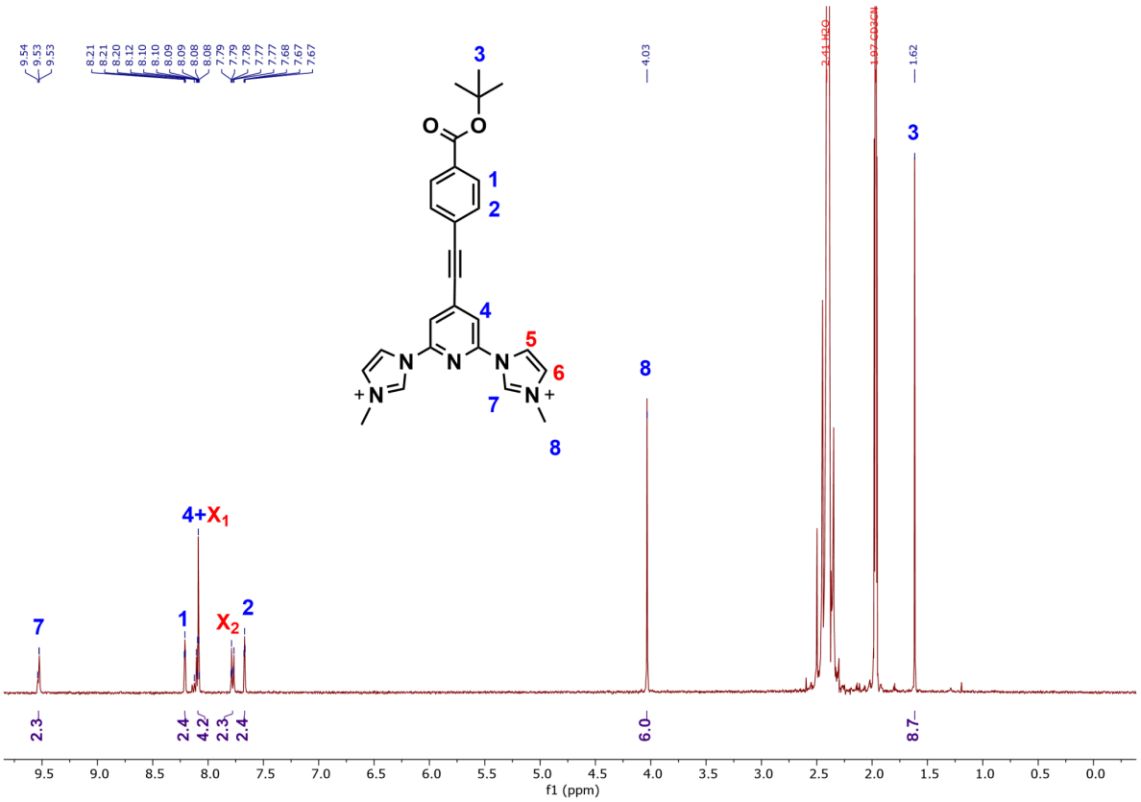

Figure A6: Proton NMR spectra of **A.V**. Protons 5 and 6 are indistinguishable in the spectra and they were thus not assigned to any specific peak, but they belong to one of the X peaks.

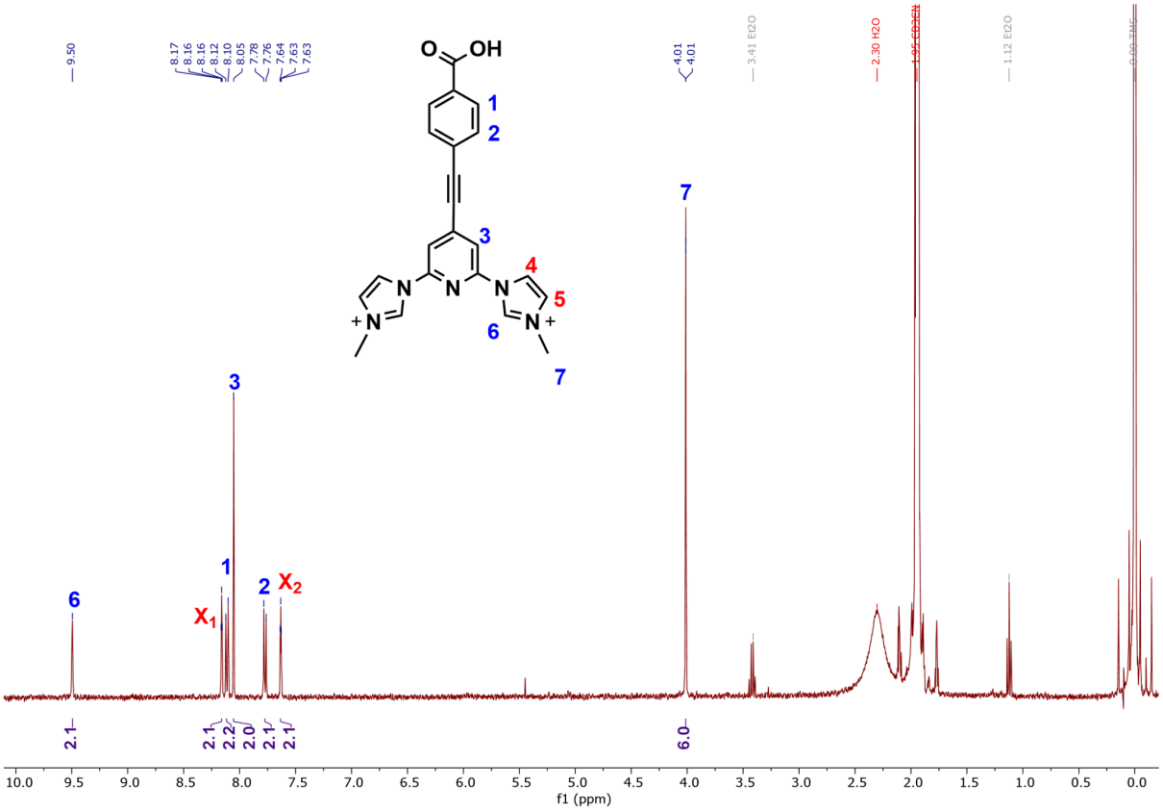

Figure A7: Proton NMR spectra of **A.VI**. Protons 4 and 5 are indistinguishable in the spectra and they were thus not assigned to any specific peak, but they belong to one of the X peaks.

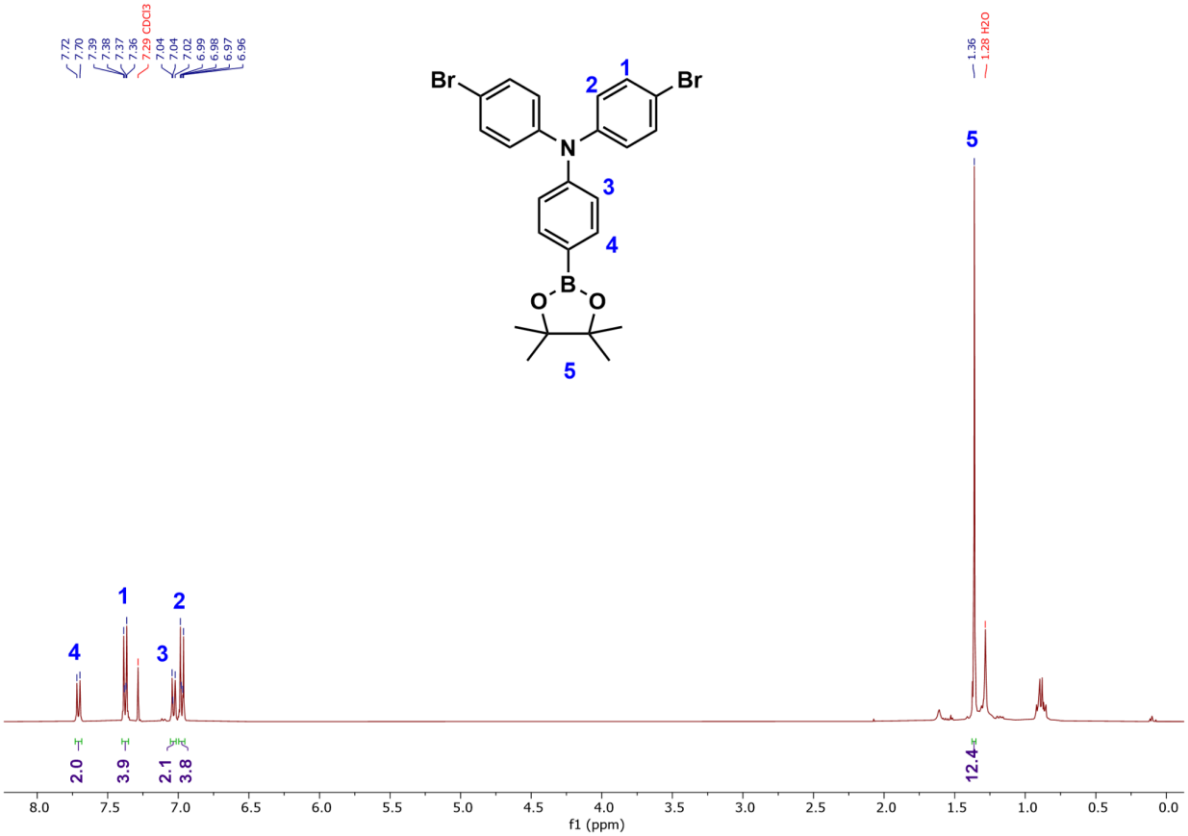

Figure A8: Proton NMR spectra of **B.I**, the numbered protons correspond to their respective peaks.

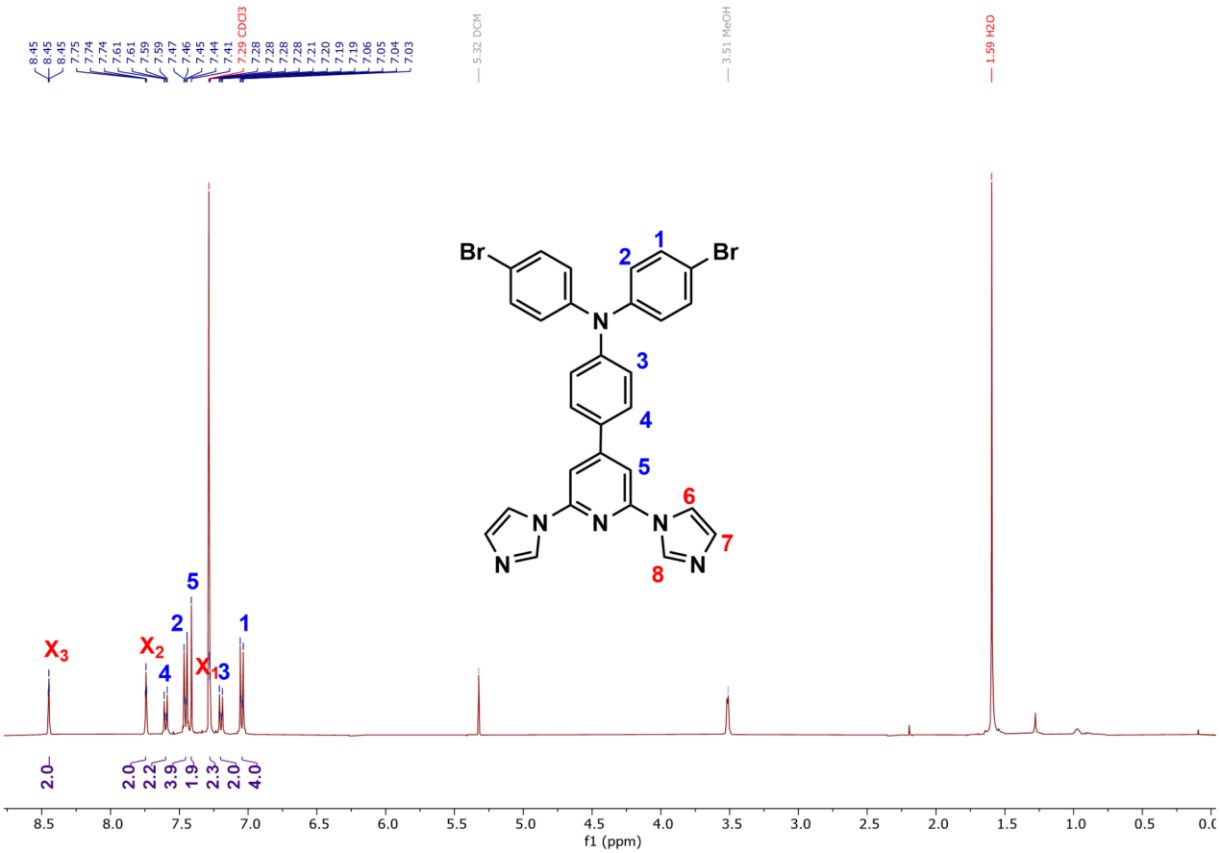

Figure A9: Proton NMR spectra of **B.II**. Protons 6, 7 and 8 are indistinguishable in the spectra and they were thus not assigned to any specific peak, but they belong to one of the X peaks.

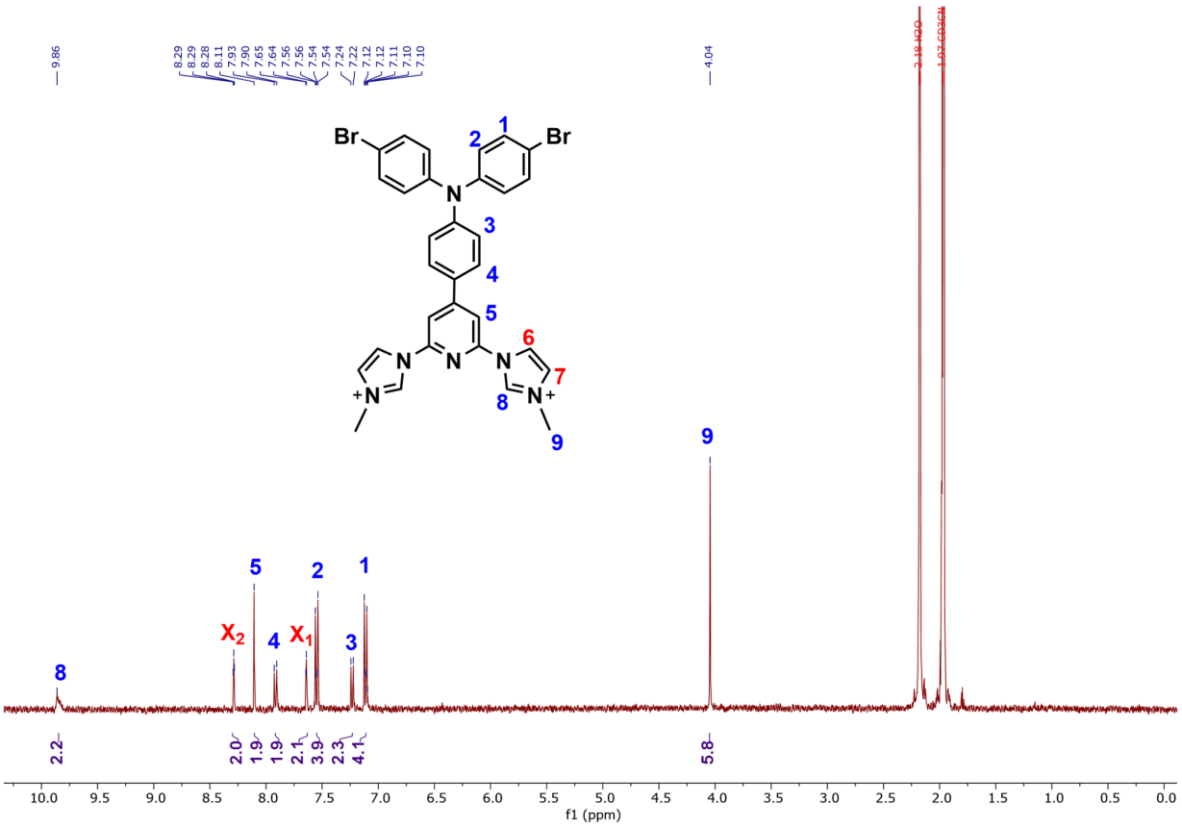

Figure A10: Proton NMR spectra of **B.III**. Protons 6 and 7 are indistinguishable in the spectra and they were thus not assigned to any specific peak, but they belong to one of the X peaks.

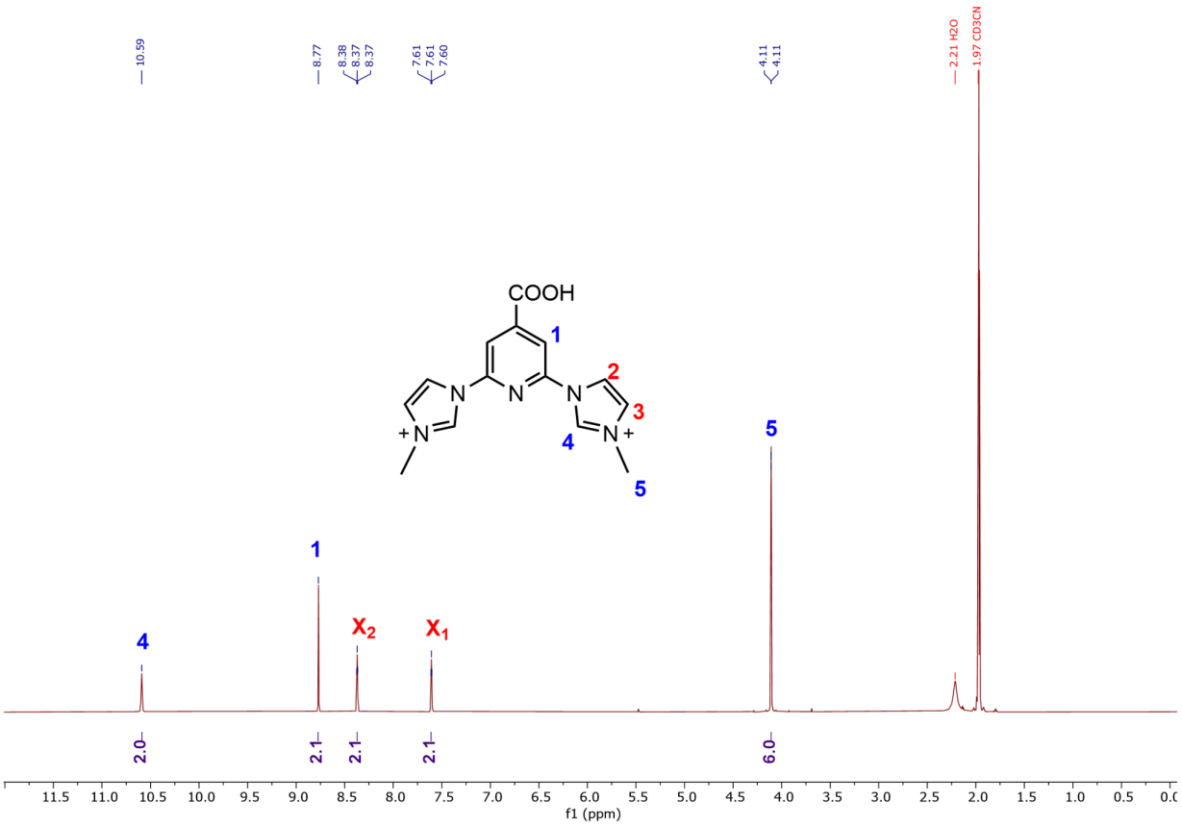

Figure A11: Proton NMR spectra of **C.I**. Protons 2 and 3 are indistinguishable in the spectra and they were thus not assigned to any specific peak, but they belong to one of the X peaks.

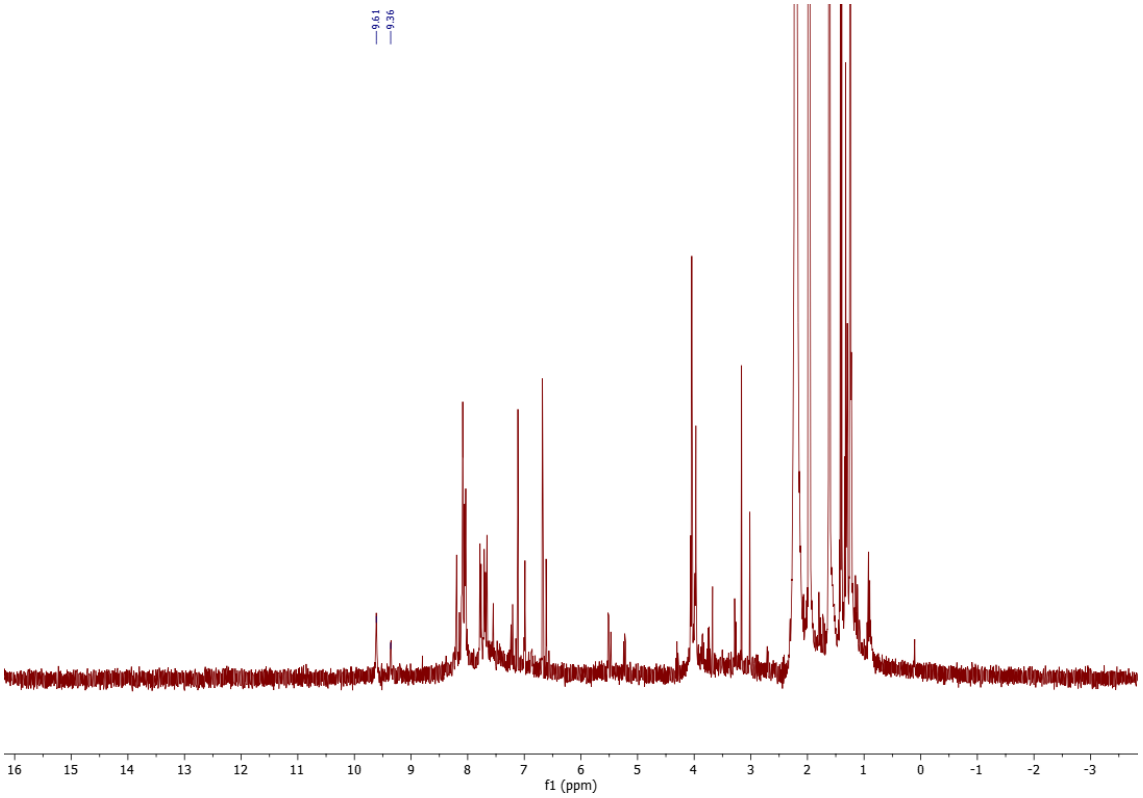

Figure A12: Proton NMR spectra of the attempt to synthesis **CX.A.V**, could not be interpreted.

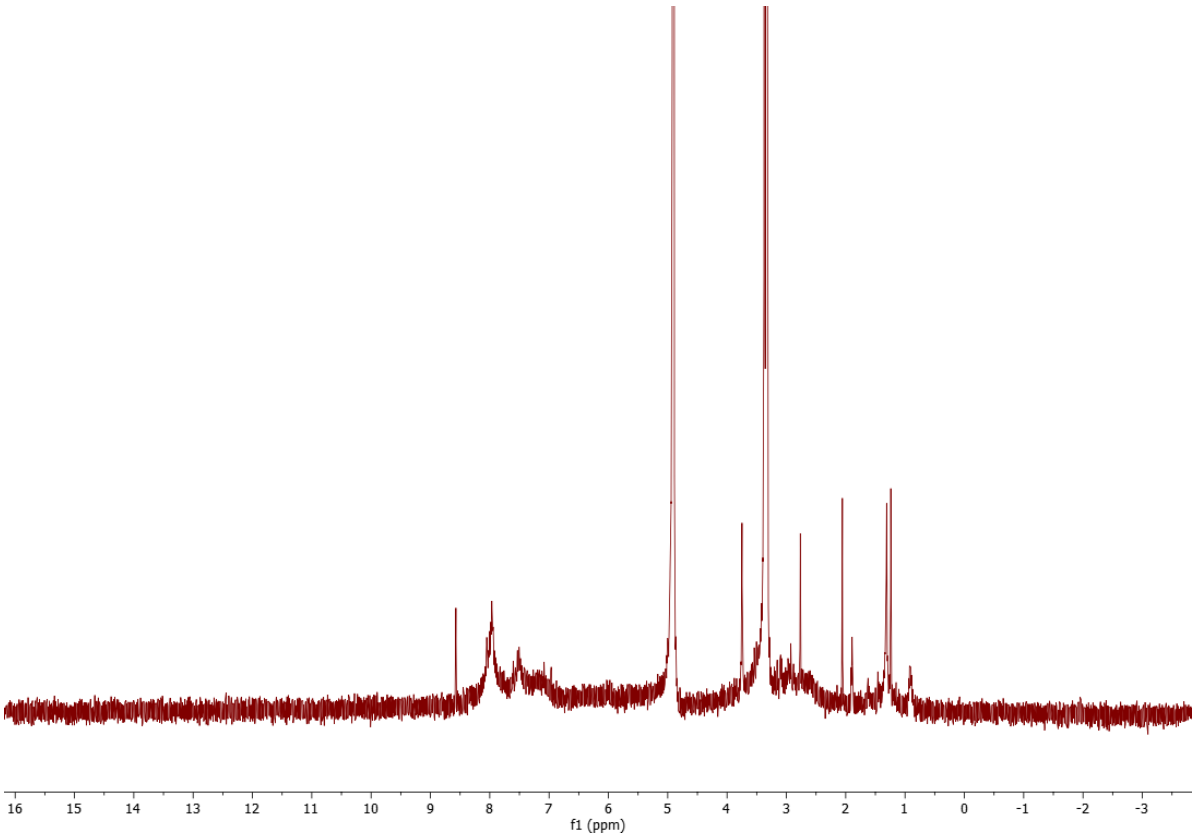

Figure A13: Proton NMR spectra of the attempt to synthesis **CX.A.VI**, could not be interpreted.

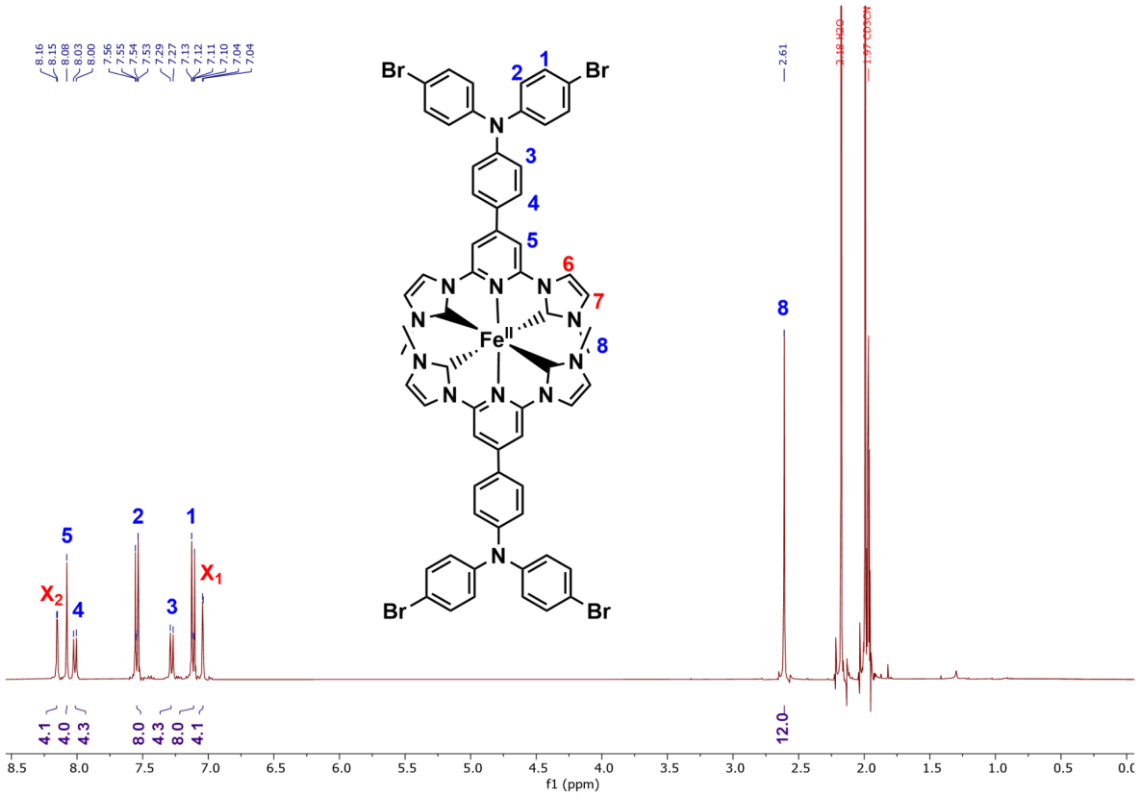

Figure A14: Proton NMR spectra of **CX.B.III**. Protons 6 and 7 are indistinguishable in the spectra and they were thus not assigned to any specific peak, but they belong to one of the X peaks.

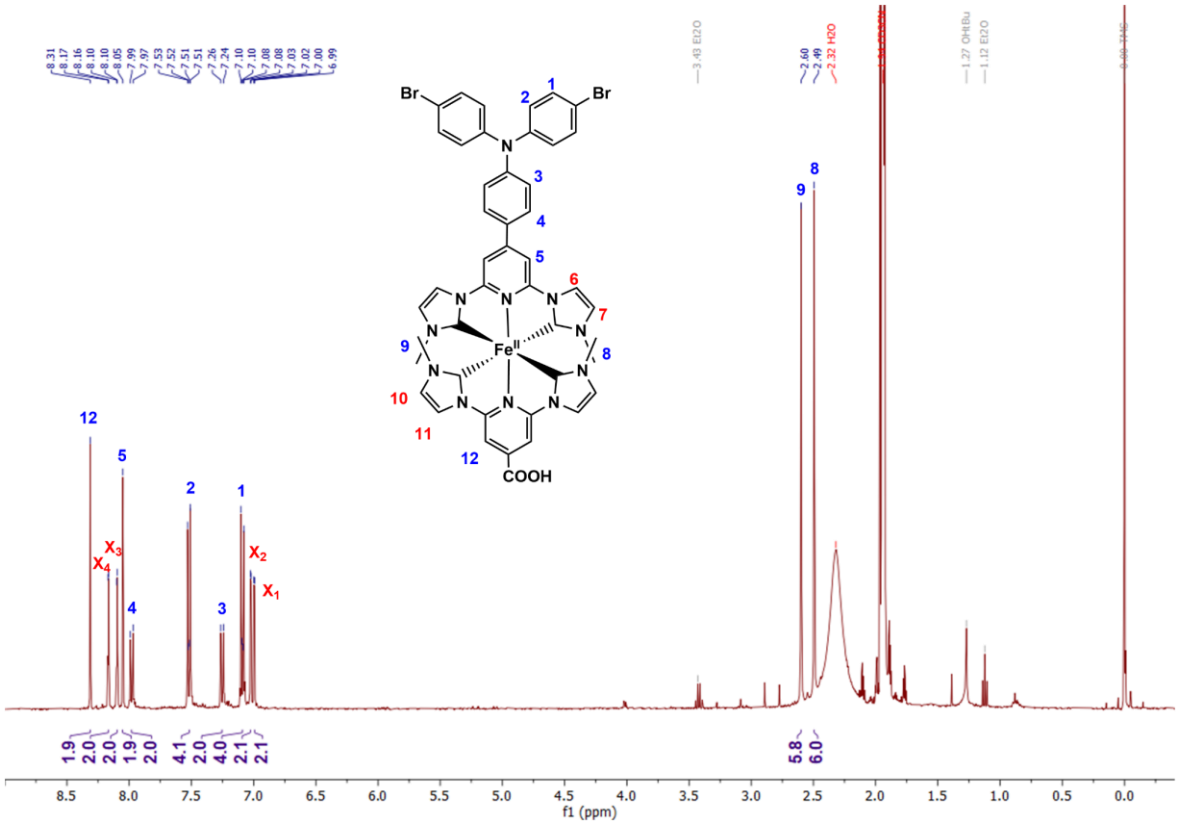

Figure A15: Proton NMR spectra of **CX.B.III.C.I**. Protons 6, 7, 10 and 11 are indistinguishable in the spectra and they were thus not assigned to any specific peak, but they belong to one of the X peaks. Protons 9 and 12 were assigned to the slightly more shifted singlet peaks due to the deshielding effect of the -COOH group.